People's Democratic Republic of Algeria

Ministry of Higher Education and Scientific Research

University M'Hamed BOUGARA - Boumerdes

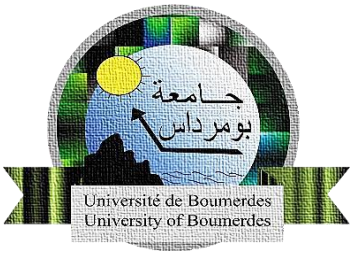

Institute of Electrical and Electronics Engineering

Department of Power and Control

Final Year Project Report Presented in Partial Fulfilment of the Requirements for the Degree of

MASTER

In: Power Engineering

Title:

MPPT Algorithms for Photovoltaic Systems under Partial Shading Conditions

Presented by:

- BENRABAH Hamza

Supervisor:

Dr. CHALAH Samira

Dr. BELMADANI Hamza

Registration Number 2024/2023

Dedication

To my Family,

You have been my unwavering source of love, support, and inspiration throughout this challenging journey. Your belief in me and your sacrifices have propelled me forward when the path seemed daunting. To my parents, who instilled in me the values of hard work and determination, and to my two brothers and one sister, who have always been my pillars of strength, I dedicate this thesis with profound gratitude and love.

To my supervisor,

Your guidance, mentorship, and patience have been invaluable. You have challenged me to push my boundaries and reach for excellence. This thesis is a testament to the knowledge and wisdom you have shared with me, and I dedicate it to you as a token of my utmost respect and appreciation.

To my Friends,

You have been my companions on this intellectual adventure, providing laughter, moral support, and a sense of belonging. Your camaraderie has made this journey not only bearable but also enjoyable. This thesis is dedicated to each of you for the countless moments of encouragement and the memories we've shared.

With heartfelt gratitude,

Hamza

Abstract

This master's thesis delves into the comprehensive study of Photovoltaic (PV) systems, focusing on various aspects critical to their efficient operation and optimization. The work is divided into five chapters, each addressing a distinct facet of PV technology and control techniques.

Chapter 1 provides a foundational understanding of PV systems, including an introduction to solar energy, photovoltaic cell technology, PV modeling, and the characteristics of solar cell I-V curves.

In Chapter 2, the focus shifts to DC-DC converters, exploring the principles and operation of Boost and Buck converters, as well as the versatile Buck-Boost inverter converter. The advantages of Boost converters are also highlighted.

Chapter 3 delves into the critical topic of Maximum Power Point Tracking (MPPT), elucidating the principles behind MPPT operation, typical MPPT-based PV system configurations, and the classification of MPPT algorithms, including indirect and direct methods.

Chapter 4 introduces soft computing algorithms and novel techniques for MPPT, including Particle Swarm Optimization (PSO), Grey Wolf Optimization (GWO), Seagull Optimization Algorithm (SOA), and the innovative Guided Seagull Optimizer. These algorithms play a pivotal role in enhancing the performance of PV systems.

Finally, in Chapter 5, the thesis presents simulation and experimental results to validate the effectiveness of the discussed algorithms under varying irradiance conditions, offering insights into their real-world applicability and performance.This research contributes to the growing body of knowledge surrounding PV systems, offering valuable insights into their operation, optimization, and control, with a particular emphasis on the application of soft computing techniques to maximize energy extraction.

Table of Contents

List of Figures :

List of Tables:

List of Acronyms

A	Diode quality factor
AC	Alternative Current
BoS	Balance of System
DC	Direct Current
DSP	Digital Signal Processor
EO	Equilibrium Optimizer
FF	Fill factor
FPGA	Field Programmable Gate Array
G	Irradiance
GWO	Grey Wolf Optimization
GMPP	Global Maximum Power Point
I	Current
IC	Incremental Conductance
I_{ph}	Photo current
I_{MPP}	Maximum Power Point Current
I_{sh}	Short Circuit Current
I_{PV}	Photovoltaic Current

K	Boltzman constant
LMPP	Local Maximum Power Point
MPP	Maximum Power Point
MPPT	Maximum Power Point Tracking
MPA	Marine Predators Algorithm
P	Power
P_{max}	Maximum Power
P_{pv}	Photovoltaic Module Power
PWM	Pulse Width Modulation
P&O	Perturb And Observe
PSO	Particle Swarm Optimization
Q	Charge of electron
R_{sh}	Shunt resistance
R_s	Series resistance
SOA	Seagull Optimization Algorithm
GSO	Guided Seagull Optimization
T	Temperature
V	Voltage
V_{MPP}	Maximum Power Point Voltage
V_{PV}	Photovoltaic Module Power
V_{OC}	Open Circuit Voltage

General Introduction

In a world where sustainable energy sources are becoming increasingly imperative, photovoltaic (PV) systems have emerged as a beacon of hope, offering a clean and renewable solution to meet our growing energy needs. Harnessing the power of the sun, these systems have revolutionized the way we generate electricity and reduce our carbon footprint. As the global transition toward green energy accelerates, understanding the intricacies of PV technology and optimizing its efficiency becomes paramount.

Another motivation that greased the wheels to a growing uptake of solar energy systems, is the emerging promising and milestone technologies that led to potential improvements to the solar cell efficiency. Nonetheless, the fluctuating nature of the generated power caused by changing atmospheric conditions throughout the day, leads to significant losses and hence a poor power conversion efficiency. Consequently, dynamic monitoring is required to detect unpredictable changes in weather conditions, and accordingly drive the operating point of the system efficiently to fully exploit the highest possible power from PV panels. The technique by which, the system is supervised and controlled to benefit from the available solar energy, to the highest extend is called Maximum Power Point Tracking (MPPT). This solution is highly cost effective and reduces the complexity of the system, instead of adding more panels and equipment which requires more area to be occupied and increases the costs substantially. The primary mission assigned to MPP trackers is to impel the operating point of the system towards its optimum point at which the power is maximum, for whatever weather conditions. This point is the peak of the nonlinear current-voltage characteristic curve of the PV panel, and it is mainly affected by the surrounding circumstances, precisely: Solar irradiance and temperature. MPPT controllers use different strategies to drive the system efficiently, classical techniques such as Perturb and observe (P&O) and Incremental conductance (IC) are widely popular due to their simplicity and ease of implementation. However, these techniques cannot handle cases at which the PV array is subjected to non-uniform solar

irradiance, this situation is known as Partial Shading Conditions (PSC) and it occurs when parts of the PV array are shaded due to certain external influences. This urged the research community to propose an enormous number of soft computing and artificial intelligence techniques to tackle the effects of partial shading conditions. Most of them have demonstrated effectiveness in dealing various situations, and they far outperform conventional methods. However, these optimizers have distinct characteristics concerning their convergence speed, robustness, efficiency and implementation complexity, and may sometimes fail under complex shading patterns. This impelled us to investigate the latest progress in the world of soft computing and metaheuristic algorithms. A survey of the some prominent and recent techniques is provided, along with their feasibility in Maximum Power Point Tracking. The main contribution of this project is to introduce the implementation of three powerful and fast novel metaheuristic algorithms: Equilibrium Optimizer (EO), Seagull Optimization Algorithm (SOA) in maximum power tracking, to drive a standalone PV system exposed to several solar irradiance levels and shading scenarios. Tracking speed and efficiency collected from various simulation tests, are the assessment parameters used to carry out the performance evaluation of the proposed optimizers.

This master's thesis embarks on a comprehensive exploration of PV systems, delving into the fundamental principles, technologies, and innovative strategies aimed at maximizing their energy production. The research is structured into five distinct chapters, each dedicated to unraveling a specific facet of PV systems and their control mechanisms.

Through this comprehensive exploration, this thesis contributes to the growing body of knowledge surrounding PV systems, offering a deeper understanding of their operation, optimization, and control. It underscores the significance of soft computing techniques in enhancing their performance and ultimately aligning our energy generation practices with a more sustainable and eco-conscious future.

Chapter 1: Generalities About Photovoltaic Systems

1.1 Introduction:

The use of solar energy is necessary in the industrial field due to its numerous characteristics, as it is an available and renewable energy. The challenge is to develop techniques to harness these energies and replace traditional energies.

The conversion of solar radiation into electricity through the photovoltaic process is one of the ways to exploit solar resources. The production of electricity through clean means has become a fundamental necessity in a world threatened by pollution and the greenhouse effect [1].

Photovoltaics **PV** is a clean and inexhaustible energy source. It represents an essential component of renewable energies that can help the world meet its ever-growing energy needs while limiting the increase in greenhouse gas emissions and reducing environmental pollution.

In other words, photovoltaics is an intermittent energy source. It is an attractive solution as a replacement or complement to conventional sources of electricity supply due to its numerous advantages [1]:

- It is a reliable means that requires little maintenance.
- It provides electricity using free and renewable solar energy.
- It does not require any fuel.
- It is silent and environmentally friendly, with no pollution.
- It has a lifespan of approximately 25 years.

In this chapter, we will present some generalities about photovoltaic systems. We will briefly describe the most commonly used solar cells and the combination of photovoltaic cells.

Next, we will present and elaborate on different models of a PV system, then select the most suitable model and describe the various equations governing it. Finally, we will simulate this model with varying sunlight and a fixed temperature, and with fixed sunlight and a variable temperature.

1.2 Solar energy

The distance from the Earth to the Sun is approximately 150 million kilometers, and the speed of light is a little over 300,000 kilometers per hour [5]. Therefore, it takes about 8 minutes for sunlight to reach us. The solar constant is the density of solar energy that reaches the outer boundary of the atmosphere facing the Sun. Its commonly accepted value is 1360 watts per square meter **W/m²**. At ground level, the density of solar energy is reduced to 1000 **W/m²** due to absorption in the atmosphere. Albert Einstein discovered, while working on the photoelectric effect, that light not only has wave characteristics but also carries energy in the form of particles called photons. The energy of a photon is given by the equation:

$$E = \frac{h \,.C}{\lambda} \qquad 1.1$$

Where:

h: Planck's constant.

C: speed of light.

Thus, the shorter the wavelength, the greater the energy of the photon [4].

A convenient way to express this energy is:

$$E = \frac{1.26}{\lambda} \qquad 1.2$$

The sun emits electromagnetic radiation, as shown in Figure (1.1), within a wavelength range ranging from 0.22 to 10 micrometers **µm** [5]. The energy associated with this solar radiation is approximately distributed as follows:

- 9% in the ultraviolet range < 0.4 **µm**
- 47% in the visible range 0.4 to 0.8 **µm**
- 44% in the infrared range > 0.8 **µm**

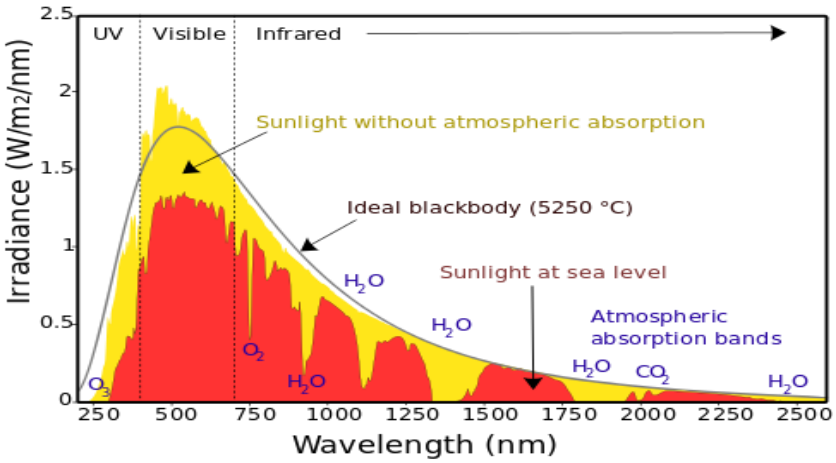

Fig. 1.1 Spectrum of Solar Radiation (Earth). [13]

1.3 Photovoltaic Cell

1.3.1 Definition

Photovoltaic cells (photon: a unit of light energy and volt: a unit of electrical potential) are electronic components made of semiconductor materials, commonly silicon in its various forms. They directly convert light energy into electricity through the photovoltaic effect. Since sunlight is the source of light energy, these cells are commonly referred to as solar cells.

1.3.2 Principle of Operation of the Photovoltaic Cell

A photovoltaic cell **PV,** also known as a solar cell, is the combination of two semiconductors, one doped P and the other doped N. At the junction of the two layers, an electric field is formed. This field exists even when the cell is in the dark. Under varying levels of sunlight, photons or light particles, carrying sufficient energy, collide with the atoms of the crystal (Figure 1.2). They are able to move the electrons from the valence band to the conduction band of the semiconductor material, thus creating electron-hole pairs. Under the influence of the potential barrier, these pairs accumulate on the outer faces of the P and N zones [2] [3].

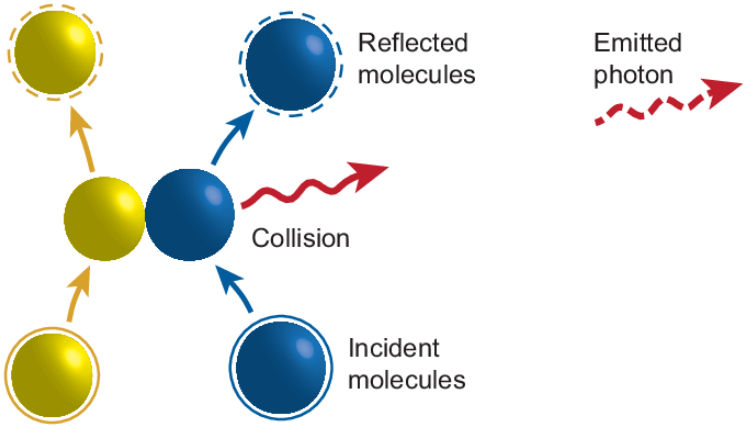

Fig. 1.2 Collision between a photon and an atom. [14]

Thus, a potential difference is created between the two faces of the cell. The metallic grids on the front and back of the PV cell collect the electrons and holes, which provide the generated electric current to an external circuit (Figure 1.3) [4]. If the photon is highly energetic, it can still only extract a single electron. The excess energy is lost as heat. The N region is covered by a metallic grid that acts as the cathode, while a metal plate (back contact) covers the other face of the crystal and serves as the anode. The total thickness of the crystal is in the order of millimeters.

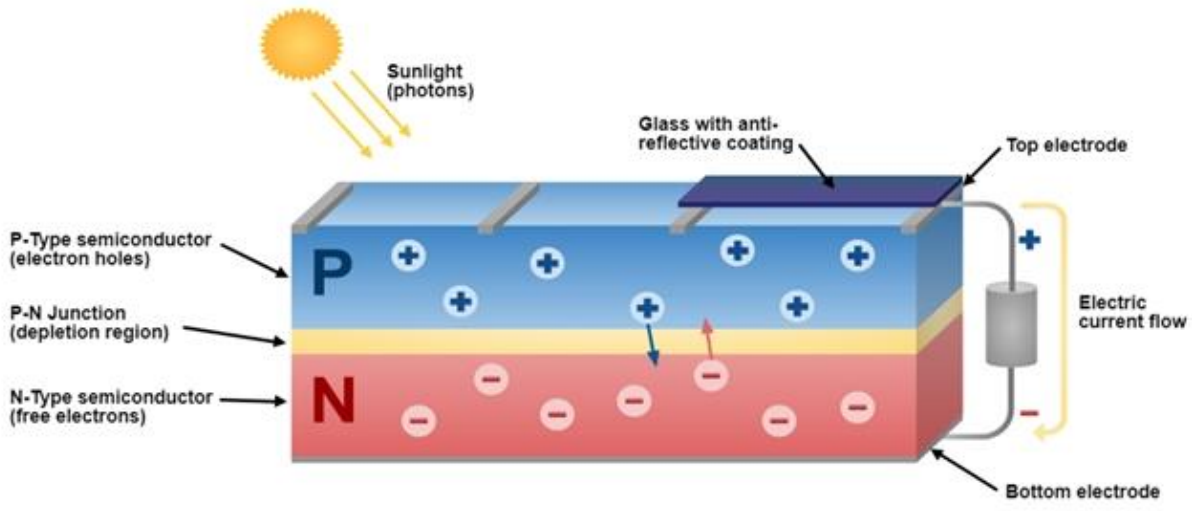

Fig. 1.3 Photovoltaic cell. [15]

1.3.3 Different types of cells

Various solar cell technologies are currently being applied and developed, with over 90% of annual solar cell production being based on crystalline silicon [6]. Based on their base material, solar cells can be divided into three groups:

- Monocrystalline silicon cells
- Polycrystalline silicon cells
- Amorphous silicon cells

Monocrystalline cells

These are the cells that have the highest efficiency (15-22%), but they also have the highest cost due to their complicated manufacturing process [7].

Polycrystalline cells

Due to their simpler manufacturing process, their production cost is lower. However, their efficiency is lower compared to monocrystalline cells (13-20%) [6].

Amorphous cells

They have a low efficiency (5%) [6], but they require very thin layers of silicon and have a low cost. They are commonly used in small consumer products such as solar calculators.

It is worth noting that regardless of the material used, the efficiency of PV conversion can reach up to 40% [6]. These low efficiencies associated with material technology represent the major challenge in harnessing solar energy [1]. Thanks to the technology of new materials such as cadmium telluride (CdTe), gallium arsenide (GaAs), and copper indium Di selenide (CIS), solar cells with laboratory efficiencies of up to 40% have been developed [1].

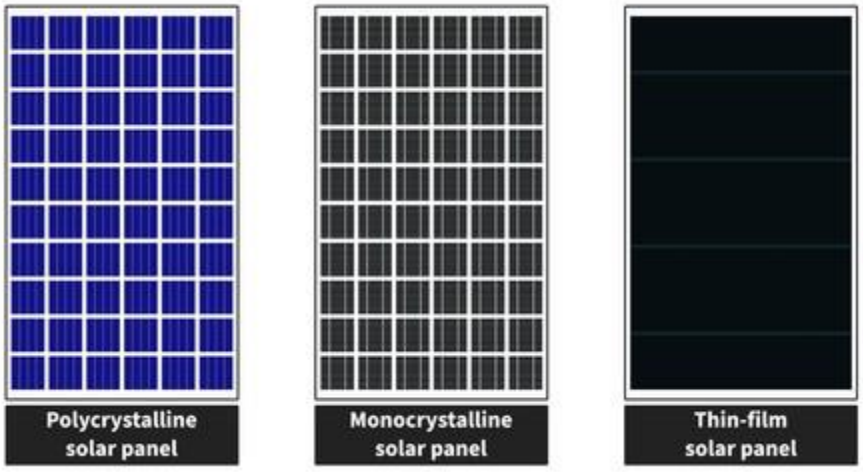

Fig. 1.4 Different types of cells.

1.3.4 The Composition of a Solar Cell

Solar radiation is transformed into direct current electricity through a photovoltaic cell, which is a semiconductor device. Since sunlight is typically a radiation source, they are commonly referred to as solar cells. Individual PV cells act as the foundational components for modules, which further serve as the building blocks for arrays and complete PV systems (refer to Figure 1.5).

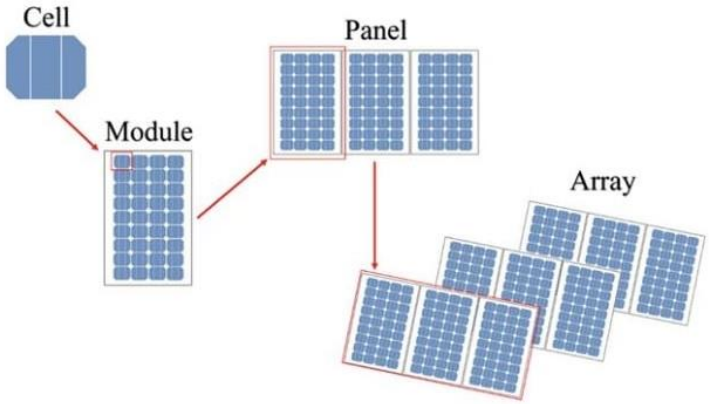

Fig. 1.5 The Composition of a Solar Cell. [16]

1.3.5 Connection of Photovoltaic Cells (The Photovoltaic Module)

The solar cell, which can be round or square in shape, is the basic building block of a solar system. A collection of cells forms a solar module, where the cells are electrically interconnected and encapsulated to protect them from external factors. Multiple modules make up a solar panel. Several panels together form a solar system or solar array, which may include additional components such as protective devices, a regulator, an energy storage system (battery), as well as monitoring and measurement devices [3].

The power provided by a single solar cell is very low, so several cells with similar characteristics need to be electrically connected and encapsulated in plastic to form a PV module. In the following, the different possible groupings of solar cells are presented.

- **Series Connection**

In a series connection, the cells are traversed by the same current, as shown in Figure 1.6. The resulting characteristic of the series connection is obtained by adding the voltages at a given current.

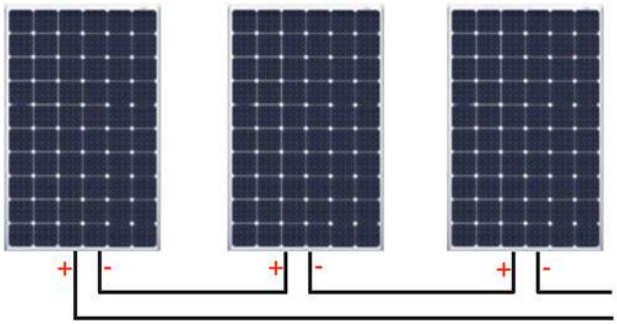

Fig. 1.6 Series Connection of cells. [17]

- **Parallel Connection**

The properties of parallel connection of cells are the dual of those in series connection. In a parallel grouping of cells, the voltage across each cell is the same, as shown in Figure 1.7 which also represents a 2 series-strings in parallel (Mixed connection).

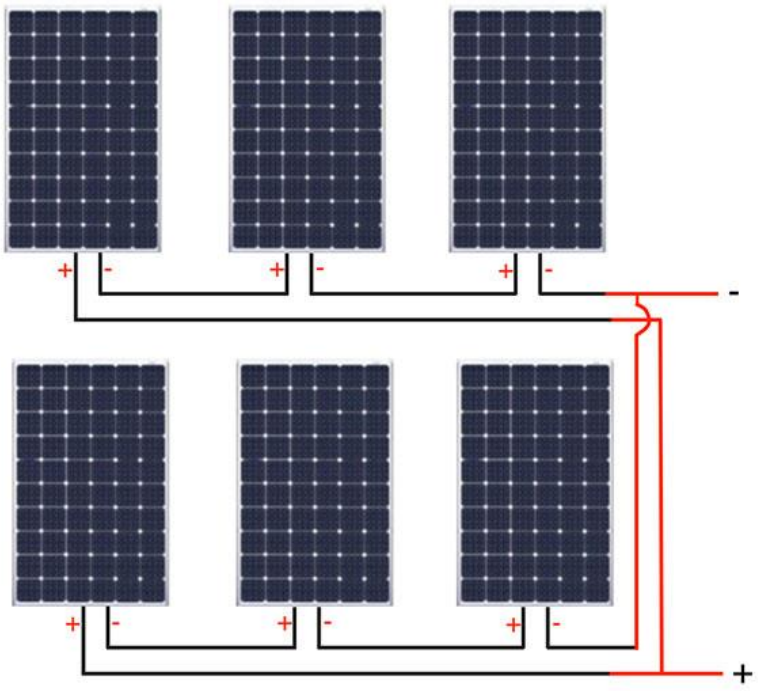

Fig. 1.7 Parallel Connection of cells. [17]

1.4 PV Modelling

1.4.1 Ideal cell

In the ideal case, a PN junction cell subjected to photovoltaic illumination and connected to a load can be represented by a current generator $\boldsymbol{I_{ph}}$ in parallel with a diode delivering current, as shown in Figure (1.8), which represents the equivalent circuit of an ideal solar cell [8].

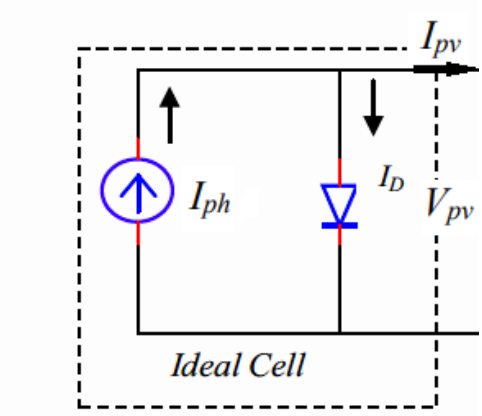

Fig. 1.8 Equivalent Circuit of Ideal Cell. [8]

The equations used in this model are:

$$I_{pv} = I_{ph} - I_d \qquad 1.3$$

The current $\boldsymbol{I_{ph}}$ is considered equivalent to the short-circuit current Isc when $\boldsymbol{V_{pv} = 0}$, which is the current obtained by short-circuiting the load.

$$I_{ph} = I_{sc} = \frac{E}{E_{ref}} \qquad 1.4$$

Where:

E: The incident light intensity absorbed by the cell.

$\boldsymbol{E_{ref}}$**:** The reference light intensity (1000 W/m²).

$$I_d = I_0(e^{\frac{V_d}{V_t}} - 1) \qquad 1.5$$

Where:

$\boldsymbol{I_0}$**:** Reverse saturation current of the diode.

$$V_t = \frac{NkT}{q} \qquad 1.6$$

Where:

$\boldsymbol{V_t}$**:** Thermal voltage.

N: Ideality factor of the photovoltaic cell.

k: Boltzmann constant $1.38 * 10^{-23}\ j/k$.

q: Charge of an electron $1.6 * 10^{-19}\ C$.

1.4.2. Real Cell

The equivalent circuit of a real photovoltaic cell takes into account the parasitic resistive effects resulting from manufacturing, as shown in Figure (1.9). This equivalent circuit consists of a diode **d** representing the junction, a current source $\boldsymbol{I_{ph}}$ representing the photocurrent, a series resistance $\boldsymbol{R_s}$ representing Joule losses, and a shunt resistance $\boldsymbol{R_{sh}}$ representing leakage current between the top grid and the back contact, which is generally much higher than $\boldsymbol{R_s}$ [9].

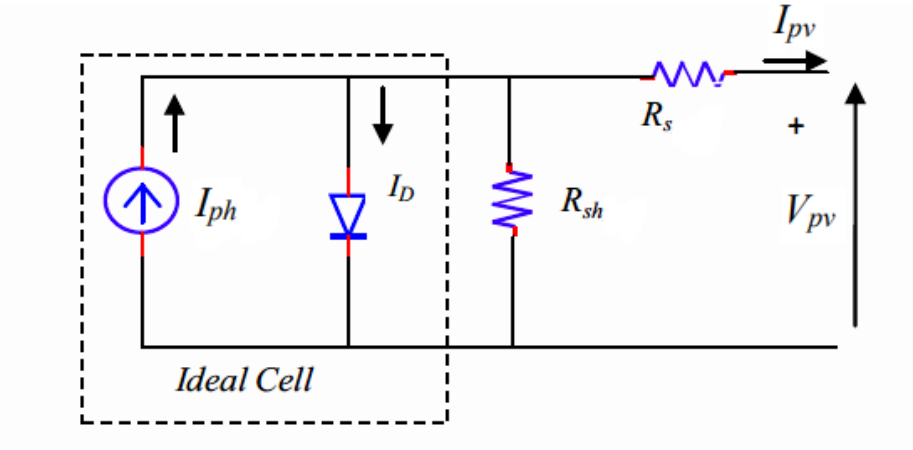

Fig. 1.9 Equivalent Circuit of Real Cell. [9]

In our work, we used the mathematical model of the solar module with a single exponential. The output current of a photovoltaic cell can be expressed mathematically as follows:

$$I_{pv} = I_{ph} - I_d - I_p \qquad 1.7$$

Where:

$\boldsymbol{I_{pv}}$**:** Current generated by the photovoltaic cell.

$\boldsymbol{I_{ph}}$**:** Photocurrent created by the cell (proportional to the incident radiation).

$\boldsymbol{I_d}$**:** Current flowing through the diode.

$$I_d = I_0(e^{\frac{V_d}{V_t}} - 1) \quad 1.8$$

$$I_0 = I_{or}(\frac{T}{T_n})^3 \, e^{\left[\frac{E_g}{BK}(\frac{1}{T_n} - \frac{1}{T})\right]} \quad 1.9$$

Where:

$\boldsymbol{I_{or}}$**:** Short-circuit current of the cell at the reference temperature Tn and reference irradiance.

T: Junction temperature of the PV cells **[K]**.

$\boldsymbol{T_n}$**:** Reference temperature of the PV cells **[K]**.

B: Ideality factor of the junction.

$\boldsymbol{E_g}$**:** Energy bandgap **[eV]**.

$$V_d = V_{pv} + R_s I_{pv} \quad 1.10$$

Where:

$\boldsymbol{R_s}$**:** Series resistance represents the bulk resistance of the semiconductor material, as well as the ohmic and contact resistances at the cell connections.

$\boldsymbol{V_{pv}}$**:** Output voltage.

$\boldsymbol{I_p}$**:** Current flowing through the $\boldsymbol{R_{sh}}$ resistor.

$\boldsymbol{R_{sh}}$**:** Shunt resistance represents the leakage around the p-n junction due to impurities and at the cell edges.

By substituting equations (1.8; 1.10) into equation (1.7), the current I_{pv} becomes:

$$I_{pv} = I_{ph} - I_0 \left(e^{\frac{V_{pv} + R_S I_{pv}}{V_t}} - 1 \right) - \frac{V_{pv} + R_S I_{pv}}{R_{sh}} \quad 1.11$$

Hence:

$$I_{ph} - I_0 \left(e^{\frac{V_{pv} + R_S I_{pv}}{V_t}} - 1 \right) - \frac{V_{pv} + R_S I_{pv}}{R_{sh}} - I_{pv} = 0 \quad 1.12$$

1.5 Solar Cell I-V Characteristic Curve

The electrical properties of PV cells are represented by a graph showing the most important parameters using the current and voltage. The next figure represents the main terms and variables concerning Solar Cell I-V Characteristic Curve.

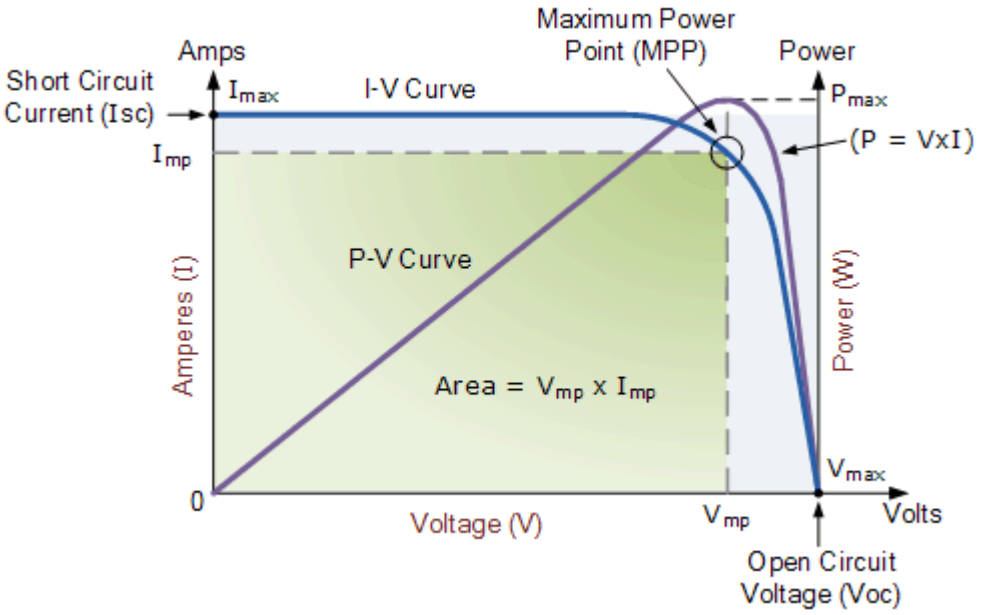

Fig. 1.10 Solar Cell I-V Characteristic Curve. [18]

- **short-circuit current Isc**

It refers to the maximum current that a PV can deliver when the solar cell is short circuited.

- **Open Circuit Voltage Voc**

It refers to the maximum voltage that a PV array can generate when the output is not connected to any load, hence no current is generated.

- **Maximum Power Point (MPP)**

It refers to the maximum power that a PV array can generate.

There are two other important parameters that are needed to evaluate the performance of the solar cells, these parameters are:

- **Power Conversion Efficiency (η)**

It refers to the proportion of solar energy received by the PV device that is successfully converted into usable electricity. It is quantified as the ratio between the output power of the solar module and the power of the incident sunlight:

$$\eta = \frac{P_{max}}{P_{In}} = \frac{V_{MPP}\, I_{MPP}}{A_c\, G} \qquad 1.13$$

Where G is the ambient radiation and AC is the cell area.

- **Fill Factor (FF)**

It is represented by a green box on the figure, the fill factor represents the actual I-V characteristic of a solar cell. A fill factor greater than 0.7 indicates a well-performing cell. However, as the cell temperature rises, the fill factor decreases [10].

$$FF = \frac{P_{max}}{V_{oc} I_{sc}} \qquad 1.14$$

1.5.1 Influence of temperature

According to the Boltzmann equation, the experience shows that the open-circuit voltage of a solar cell decreases with an increase in cell temperature [11,12].

In Figures 1.11 (a and b), we present the I-V and P-V characteristics of a 2500 photovoltaic module for a given sunlight level (G) and different temperatures.

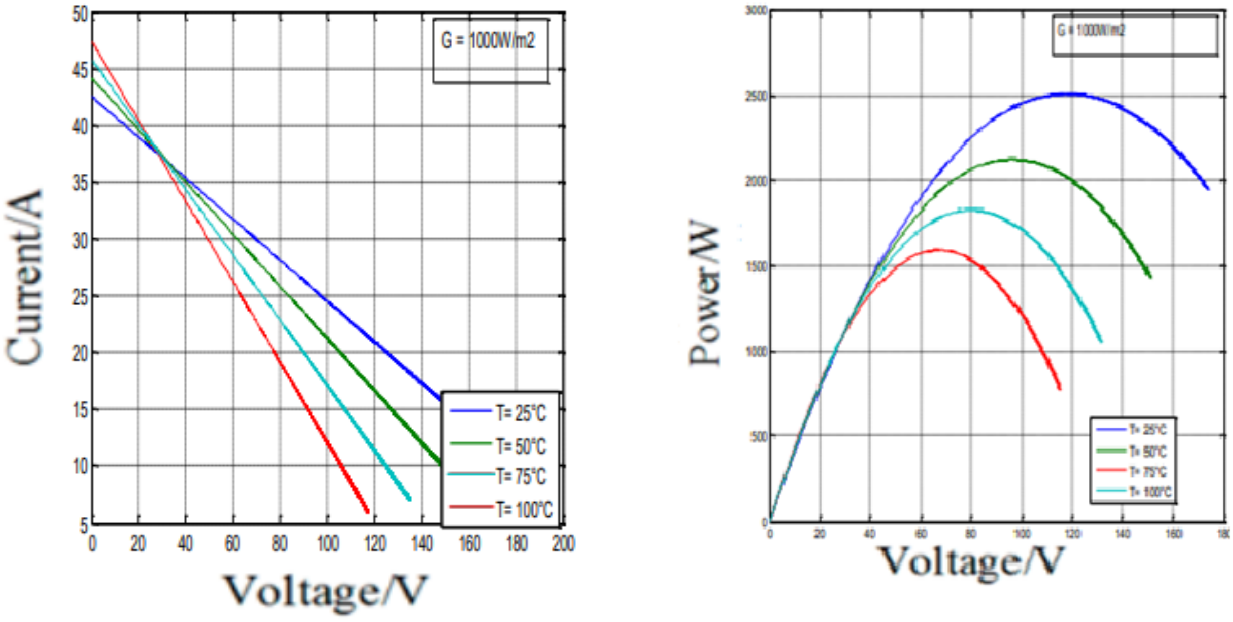

A **B**

Fig. 1.11 A) I-V characteristics, B) P-V characteristics – with influence of temperature.

We notice that the current depends on temperature as it slightly increases with temperature. However, we observe that the temperature has a negative effect on the open-circuit voltage. As the temperature increases, the open-circuit voltage decreases. On the other hand, the maximum power of the generator decreases as the temperature increases (Figure 1.11 b).

1.5.2 Influence of irradiance

We have kept the temperature constant for different irradiance levels Figure 1.12 (a and b).

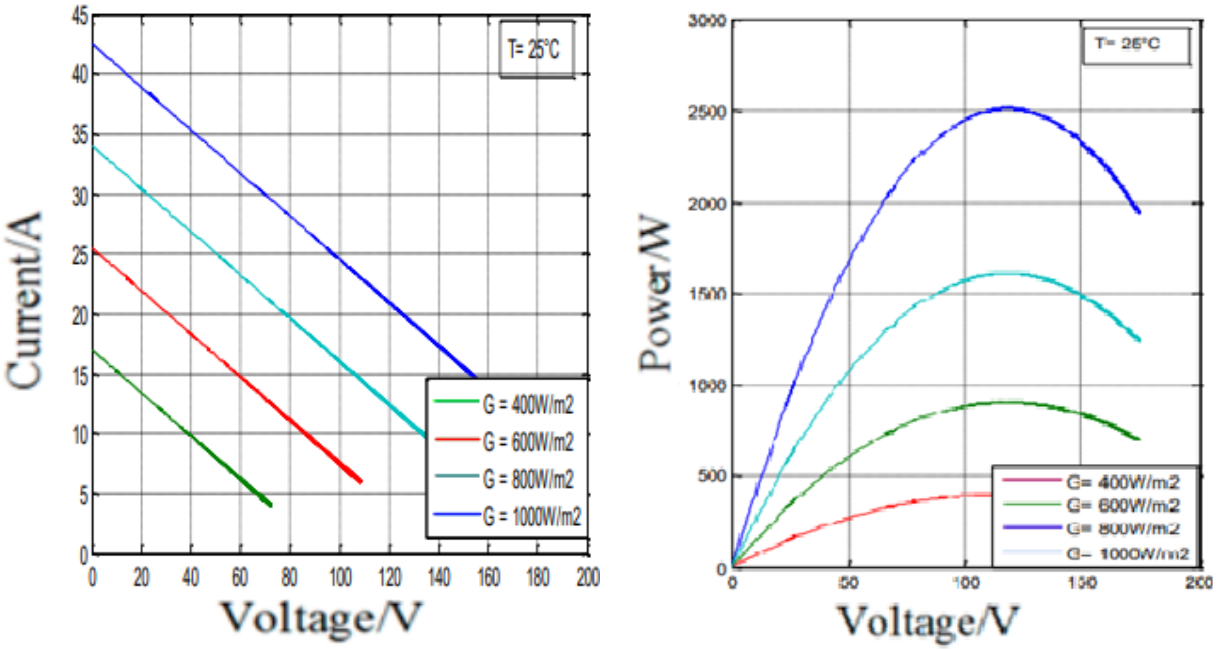

A **B**

Fig. 1.12 A) I-V characteristics, B) P-V characteristics – with influence of irradiance.

In Figure **A**, we observe that for an irradiance of **G** = 1000 **W/m2**, the short-circuit current **Isc** is **42A**, and for **G** = 800 **W/m2**, **Isc** is **33A**. We can see that the current undergoes a significant variation, increasing as the irradiance increases. However, the voltage varies slightly. This results in an increase in power when the irradiance is increased, as shown in Figure **B**.

1.6 Conclusion

In this chapter, we have presented the main characteristics and technologies of the components of a PV generator. We have also shown how to increase the current or voltage of a photovoltaic generator, as well as the influence of temperature and irradiance on cell efficiency. We have observed that power depends not only on temperature but also on irradiance.

For the optimal operation of a photovoltaic system, it is necessary to use a matching stage between the PV generator and the load, or another system that we will study in the next chapter.

Chapter 2: DC – DC Converters

2.1 Introduction:

For power conversion, it is essential to maintain high efficiency to avoid power dissipation and excessive heating in electronic components. For this reason, all power conversion takes place around energy storage components (inductors and capacitors) and switches. The choice of power switches depends on the power level to be converted or controlled. MOSFETs (Metal-Oxide-Semiconductor Field-Effect Transistors) are typically used for relatively low power levels (a few kW), while IGBTs (Insulated Gate Bipolar Transistors) are employed for higher power levels. Thyristors have traditionally been used and accepted for the highest power levels [19].

The DC-DC converter is a power electronics device that utilizes one or more controlled switches to modify the voltage value of a DC voltage source with high efficiency.

The switching operation is performed at a high frequency. If the output voltage is lower than the input voltage, the converter is called a step-down converter (or buck converter). Conversely, if the output voltage is higher, it is referred to as a step-up converter (or boost converter). There are converters capable of operating in both directions (boost-buck).

Some converters are also reversible, meaning they can provide energy back to the source. There are different classification methods for DC-DC converters. One of them depends on the isolation property between the primary and secondary sides. Isolation is typically achieved using a transformer, which has a primary side on the input and a secondary side on the output. The feedback loop for control is established through another smaller transformer or optically through an optocoupler. As a result, the output is electrically isolated. From the input. This type includes converters (Fly-back) with an additional AC-DC rectifier bridge at the front. However, due to the bulky and costly implementation of these transformers, non-isolated DC-DC converters are more preferred [20].

Non-isolated DC/DC converters can be classified as follows:

2.2 Boost Converter

2.2.1 Boost Converter Circuit

A Boost converter, or parallel chopper, is a switching power supply that converts a DC voltage into another DC voltage of higher value. Figure 2.1 shows the basic circuit diagram of a Boost converter.

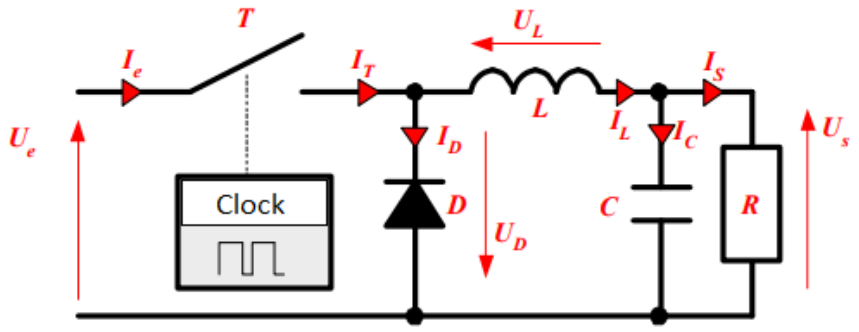

Fig. 2.1 Block diagram of a Boost type step-up converter.[21]

2.2.2 Operating principle

The converter can operate in two modes depending on its energy storage capacity and the switching period **T**.

These two operating modes are:

- **Continuous mode**: In this case, the energy stored in the inductance **L** is partially transferred, and therefore the current in the inductance does not reach zero.

- **Discontinuous mode**: In contrast, in this case, the energy stored in the inductance **L** is completely transferred, and therefore the current in the inductance reaches zero.

In our work, the study of operation is based on the continuous conduction mode. The circuit operation can be divided into two intervals according to the switching interval (**Ton**, **Toff**).

The **Ton** interval starts when the transistor **Q** is closed at **t = 0**. The input current, which rises, flows through the inductance **L** and the transistor.

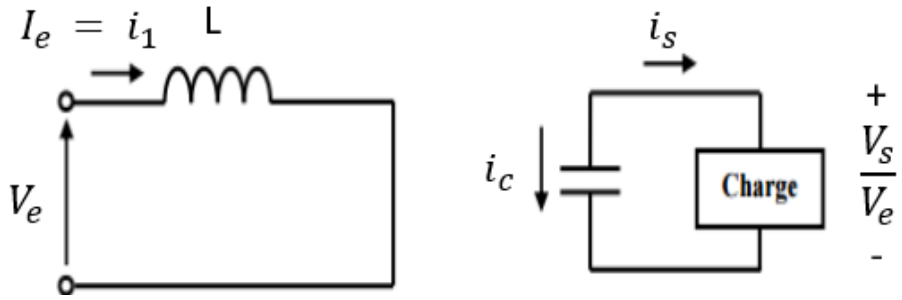

Fig. 2.2 Equivalent circuit for Ton. [21]

The **Toff** interval begins when the transistor **Q** is opened at **t = t1**. During this interval, the current in the inductor starts to decrease as the energy stored in the inductance **L** is transferred to the load (Figure 2.3).

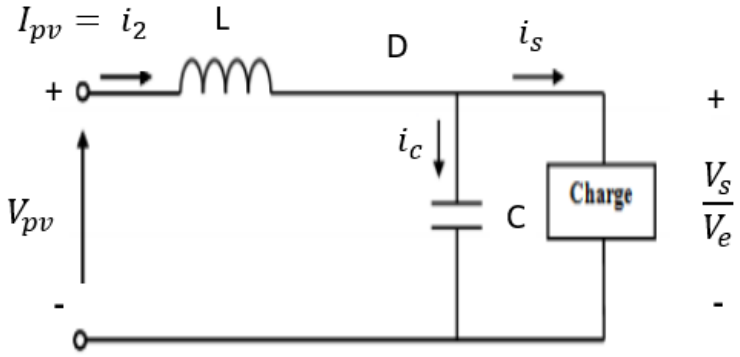

Fig. 2.3 Equivalent circuit for Toff. [21]

In the **Ton** interval, the current of the inductance is given by: $V_e = V_{pv}$

$$V_e = L \frac{di}{dt} \qquad 2.1$$

$$i_1 = \frac{V_e}{L} t + I_m \qquad 2.2$$

Figure 2.4 represents the current curve through the inductance in the **Ton** and **Toff** intervals. Where **I1** is the current at the initial instant. During this interval, the current through the inductance increases.

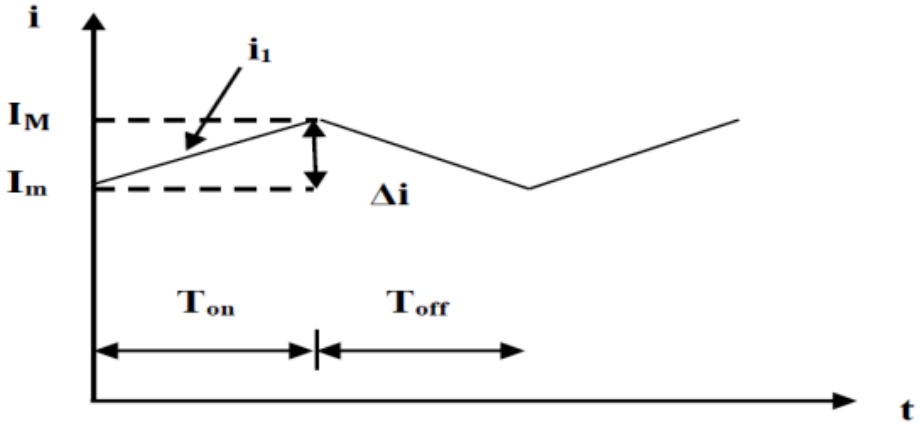

Fig. 2.4 Current waveform. [21]

In continuous conduction mode, the switching period is **T** = **Ton** + **Toff** and the duty cycle is:

$$\alpha = \frac{Ton}{T} \qquad 2.3$$

On the other hand, we can express the output voltage in terms of the input voltage and the duty cycle as follows:

$$V_s = \frac{1}{1-\alpha} V_e \qquad 2.4$$

For the Boost converter:

$$V_s > V_{pv} \ \forall \alpha \ and \ 0 < \alpha < 1 \qquad 2.5$$

We can vary the output voltage of the converter by changing the duty cycle value **α**.

The output voltage is minimum when **α = 0**. We cannot have **α = 1**, which would correspond to a continuously closed switch. For **α** close to **1**, the output voltage becomes very high and highly sensitive to changes in the duty cycle **α**. Additionally, the influence of losses in the circuit limits the maximum output voltage of the converter.

The voltage gained theoretically tends to infinity for a unity duty cycle if we consider the circuit without losses. In summary, we can express the steady-state output voltage and current as follows:

$$V_s = \frac{V_{pv}}{1-\alpha} \qquad 2.6$$

$$i_s = (1-\alpha)\, i_{pv} \qquad 2.7$$

The figure (2.5) located below represents the different curves of the electrical quantities.

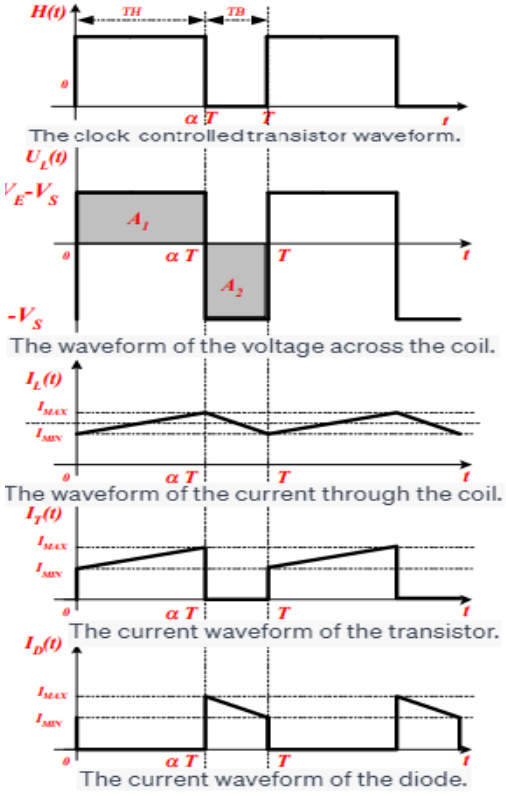

Fig. 2.5 Timing diagrams of the Boost converter. [21]

2.3 Buck Converter

2.3.1 Schematic of the converter

Figure 2.6 represents the basic schematic of a Buck converter.

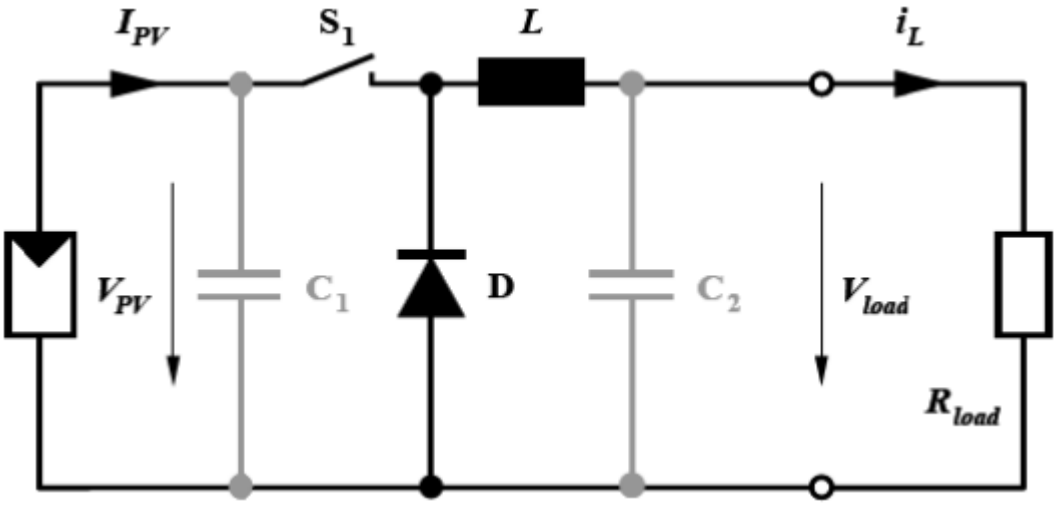

Fig. 2.6 Electronic schematic of a Buck converter. [22]

2.3.2 Operating principle

A Buck converter, also known as a step-down converter or series chopper, is a switching power supply that converts a continuous voltage into another continuous voltage of lower value. This type of converter can be used as a source-load adapter when the operating point in direct coupling is to the left of the Maximum Power Point (**MPP**).

If the switch **S1** is activated at **t0**, a current flow through the circuit but does not pass through the diode **D** since it is reverse-biased. The current $\boldsymbol{I_L}$ does not increase immediately but rather linearly with a growth rate determined by the inductance **L** [23,22].

$$\frac{di_L}{dt} = \frac{V_{pv} - V_{Load}}{L} \qquad 2.8$$

$$I_L = \left(\frac{V_{pv} - V_{Load}}{L}\right) t + I_m \qquad 2.9$$

During this time, the inductance stores energy in the form of a magnetic field. If **S1** is deactivated after **t = t1**, the load is disconnected from its power supply. However, the current is maintained by the energy stored in the inductance **L** and flows through the diode **D**, also known as a "freewheeling diode." This diode allows the energy stored in the inductance to be dissipated when the switch opens without creating overvoltage. According to equation (2.8), the current decreases, since:

$$\frac{di_L}{dt} = -\frac{V_{Load}}{L} \qquad 2.10$$

$$I_L = \left(-\frac{V_{Load}}{L}\right) t + I_m \qquad 2.11$$

The figures (2.7) and (2.8) depict the on-state and off-state circuit of the Buck converter, respectively.

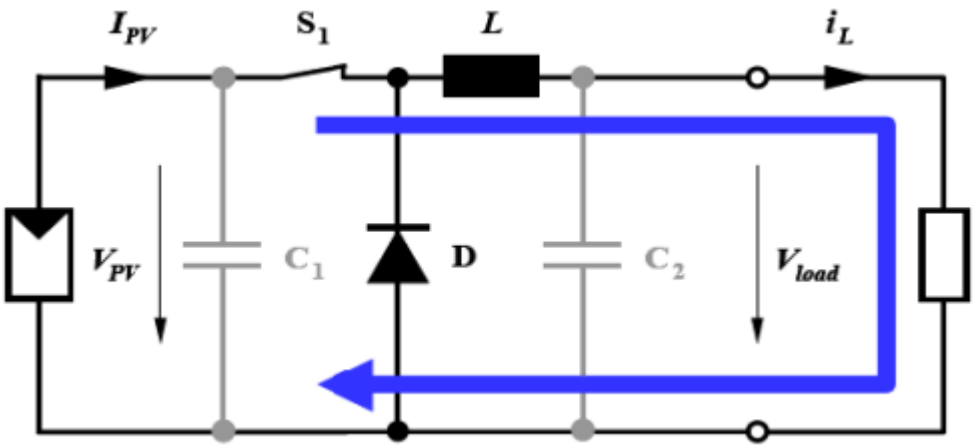

Fig. 2.7 Buck Converter in the ON state.

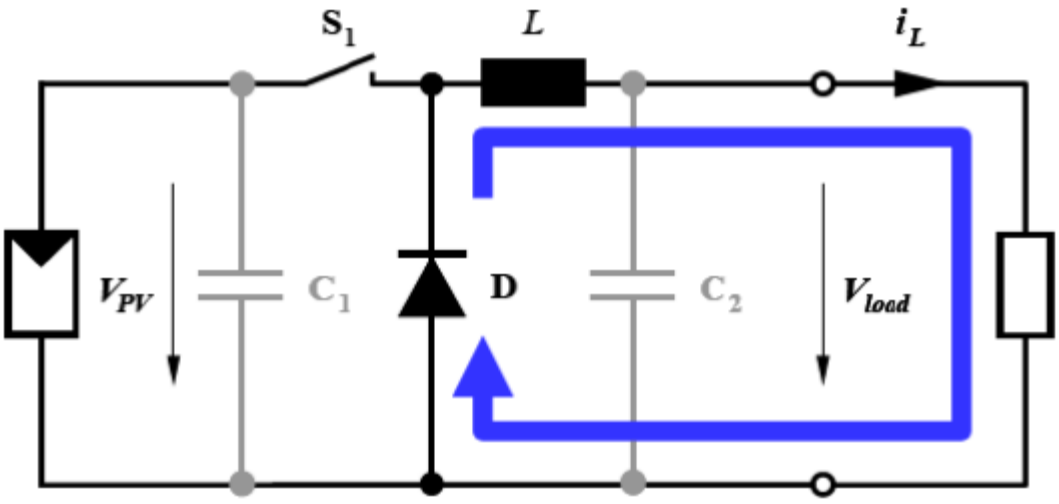

Fig. 2.8 Buck converter during the Off state. [22]

The capacitor **C1** helps reduce the peaks of the current drawn from the **PV** generator, support the **PV** voltage, and attenuate noise. The switch **S1** is turned on and off at a switching frequency **f = 1/T**. The voltage across the load exhibits ripple, which can be smoothed by adding a capacitor **C2**. However, the average value $\boldsymbol{V_{Load}}$ is lower than $\boldsymbol{V_{pv}}$. In the case where the frequency is increased, for example, to several **KHz**, the required inductance can be significantly reduced. The voltage across the load is given by:

$$V_{Load} = \frac{Ton}{T} = \alpha V_{pv} \qquad 2.12$$

With **T = Ton + Toff**, which is the switching period.

$\frac{Ton}{T} = \alpha$ is the duty cycle ($0 < \alpha < 1$)

With this equation, we can see that the output voltage varies linearly with the duty cycle. Here, we are considering only the behavior of the circuit in continuous conduction mode (**CCM**). It should be noted that the switch used is a semiconductor device in switching operation. Typically, a **MOSFET** transistor is used for its low switching time in order to minimize power losses.

2.4 Inverter converter "BUCK - BOOST"

2.4.1 Converter schematic

Figure 2.9 represents the basic schematic diagram of a Buck-Boost converter.

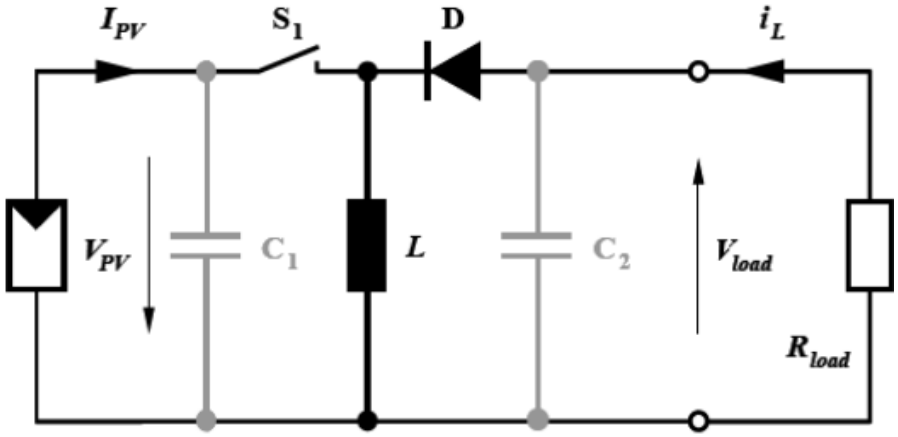

Fig. 2.9 Schematic diagram of the Buck-Boost inverter converter. [22]

2.4.2 Operating Principle

A Buck-Boost converter is a switching power supply that converts a **DC** voltage into another **DC** voltage of lower or higher value but with opposite polarity. During the "**ON**" state, energy is supplied by the source.

The energy provided by the **PV** source (generator) is stored in the inductance **L** during the "**ON**" state (Figure 2.10). The energy stored in the inductance **L** is then delivered to the load during the "**OFF**" state (Figure 2.11). Due to the presence of the diode **D**, the current flows through the inductance L in only one direction during both states. Therefore, **V1** has a polarity opposite to $\boldsymbol{V_{pv}}$. For this reason, this circuit is also called an inverting converter. The equations describing this circuit can be obtained in the same way as before. As mentioned earlier, capacitor **C1** supports the $\boldsymbol{V_{pv}}$ supply voltage, while **C2** soothes the load voltage. In conclusion, the amplitude of $\boldsymbol{V_{Load}}$ can be lower or higher than VPV depending on the values of **Ton** and **Toff** [24].

$$V_{Load} = -\frac{Ton}{T} V_{pv} = \frac{\alpha}{1-\alpha} V_{pv} \quad 2.13$$

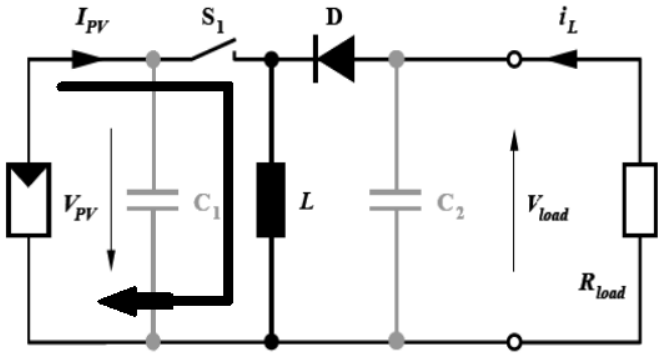

Fig. 2.10 Buck-Boost Converter during the ON state.

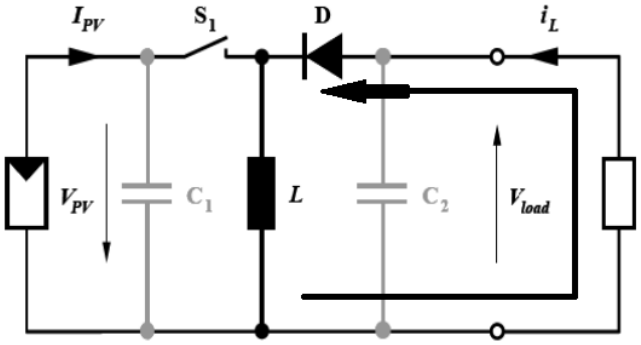

Fig. 2.11 Buck-Boost Converter during the OFF state. [22]

In all three cases mentioned above, the matching between the source and the load is achieved by choosing appropriate values of the duty cycle. Generally, for **DC/DC** converters, the switch is controlled by a **PWM** (Pulse Width Modulation) signal. A **PWM** signal is a rectangular waveform with a fixed frequency but a variable duty cycle **α**. The duty cycle value determines the amount of time.

2.5 Analysis and selection of the converter

A **PV** solar panel is a low-voltage **DC** electricity generator. It is preferable to use a voltage boosting device such as a boost converter as an adapter stage. Impedance matching between the source and the load is desirable. All the converters mentioned earlier, except for the Buck

converter, can serve as voltage-boosting devices. In fact, the Buck-Boost structure acts as a voltage booster when the duty cycle is greater than one-half. In terms of complexity, the Boost converter is the simplest. The voltage and current constraints on the switches and diodes are nearly similar for different voltage-boosting topologies.

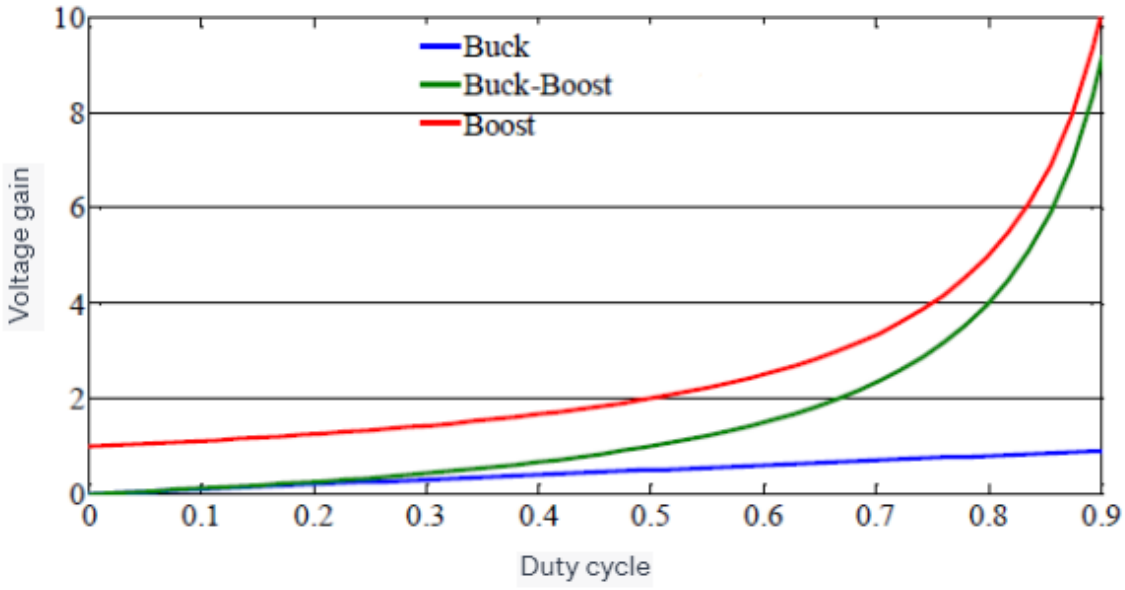

Fig. 2.12 Voltage gain evolution as a function of the duty cycle for the converters.

If we compare them in terms of voltage gain, the Boost converter takes the first place, as shown in Figure 2.12, which shows the voltage gain evolution as a function of the duty cycle. Furthermore, it can also be noticed that the diode **D** present in the Boost converter can act as protection for the **PV** generator, eliminating the need for a freewheeling diode and resulting in cost savings compared to other topologies [25].

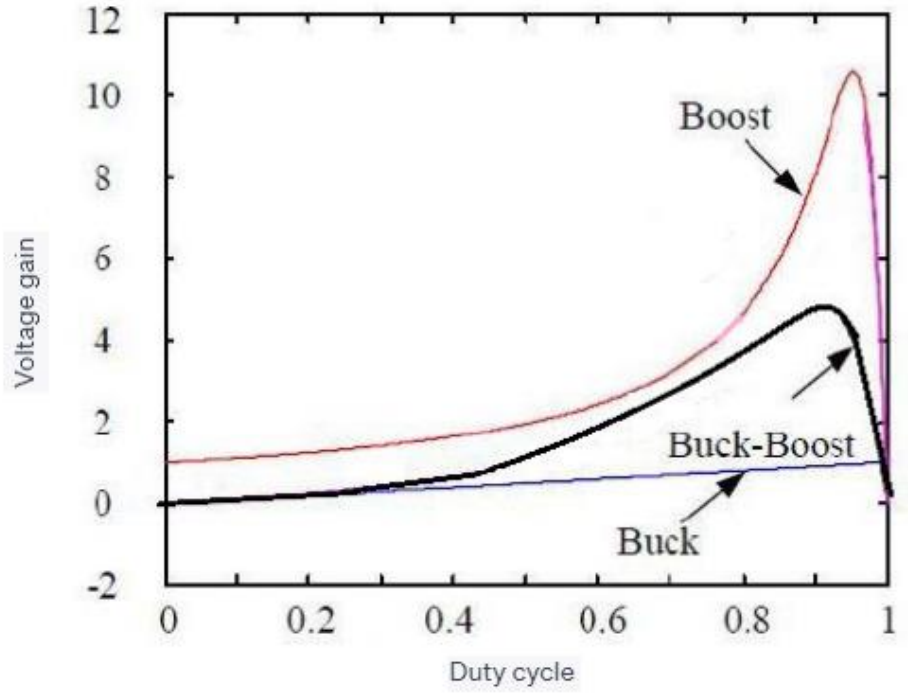

Fig. 2.13 Evolution of voltage gain taking into account the parasitic elements of the converters.

2.6 Advantages of the Boost converter

Despite the high efficiency of the Buck converter in systems with conventional power sources, the Boost converter may be more suitable for photovoltaic systems with maximum power point tracking (**MPPT**) since the converter operates in continuous current mode, extracting as much power as possible from the solar cells. Therefore, the energy efficiency of the Boost converter can be greater than that of the Buck converter. The Boost converter is generally used to obtain a higher output voltage, while the Buck converter is used to lower the output voltage [26].

2.7 Conclusion

In this chapter, we briefly discussed some commonly used switching converter topologies (Buck, Boost, and Buck-Boost) in photovoltaic systems for generating desired voltages and currents, as well as for adapting solar panels to different loads.

These types of converters are composed only of reactive elements (inductors, capacitors) which, in the ideal case, consume no energy. This is why they are characterized by high efficiency. Each topology we studied has its advantages and disadvantages. However, considering the application or system being studied, the Boost converter stands out as the best choice due to its voltage boosting capability, high efficiency, and circuit simplicity.

CHAPTER 3 : MAXIMUM POWER POINT TRACKING

3.1 Introduction

The operating power of solar panels is easy to calculate. It is equal to the product of voltage and current. However, determining the reference power is more challenging as it depends on meteorological parameters such as temperature and irradiance. This variable reference power, characterized by a nonlinear function, makes achieving maximum power operation more difficult. Therefore, a control technique for Maximum Power Point Tracking (**MPPT**) is necessary. This **MPPT** algorithm can range from simple to complex and is typically based on adjusting the duty cycle of the static converter until it reaches the Maximum Power Point (**MPP**).

In this chapter, we will see an introduction to the **MPPT** and its basic principle of working and study some classic techniques for tracking the operating point of a photovoltaic generator.

3.2 The principle of operation of MPPT

An **MPPT** (Maximum Power Point Tracker) is a control system associated with a **DC-DC** converter stage that allows the photovoltaic generator to operate at its maximum power output continuously. The control technique involves adjusting the duty cycle automatically to bring the generator to its optimal operating point, regardless of meteorological instabilities or sudden load variations that may occur at any time.

Figure 3.1 illustrates three cases of disturbances. Depending on the type of disturbance, the operating point shifts from the maximum power point (**MPP**) to a new operating point (**P**) that may be closer or further away from the optimum.

As shown in Figure 3.1, for an incident power level (**E1**), the optimal power transferred to the load occurs at the **MPP1**. If the incident power changes (**E2**), then the new maximum power point becomes **MPP2**, and the operating point of the **PV** generator shifts to **P1**. By readjusting the duty cycle value, the system can converge towards the new maximum power point (**MPP2**).

To a lesser extent, a variation in the operating point can also occur due to changes in the operating temperature of the **PV** generator (Case B). In this case, adjustments at the control level are necessary. Similarly, when the load changes (Case C), the operating point may shift, but it can be brought back to a new optimal position through the action of the control system.

In summary, tracking the **MPP** is achieved through a specific control system called **MPPT**, which primarily adjusts the duty cycle of the static converter (**SC**) to search for and reach the **MPP** of the **PV** generator.

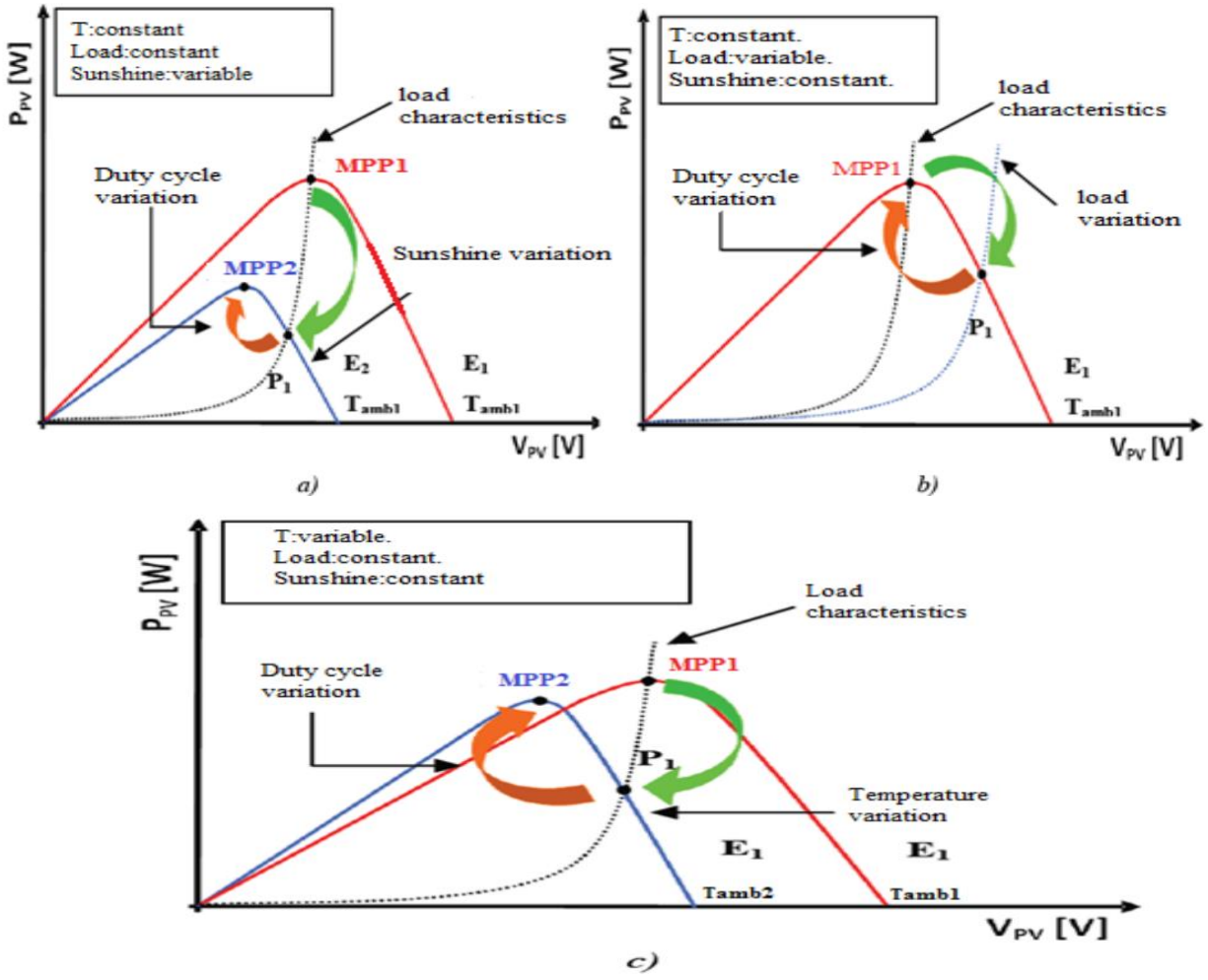

Fig. 3.1 The variation of the Maximum Power Point (MPP) with respect to irradiance, temperature, and load. [27]

3.3 Typical MPPT based PV system.

An example of a **PV** system utilizing **MPPT** technology is depicted in figure 13. Solar panels convert sunlight into electrical energy based on the intensity of light they receive. This generated power is directed to a **DC-DC** converter, which is controlled by an **MPPT** controller that continuously monitors the real-time parameters of the solar panel, specifically its voltage and current. Using the gathered data and its internal algorithm, the **MPPT** tracker calculates the necessary modifications to the duty cycle of the power converter. This enables the system to find and maintain the Maximum Power Point (**MPP**) that aligns with the current operating conditions, ensuring the system operates optimally.

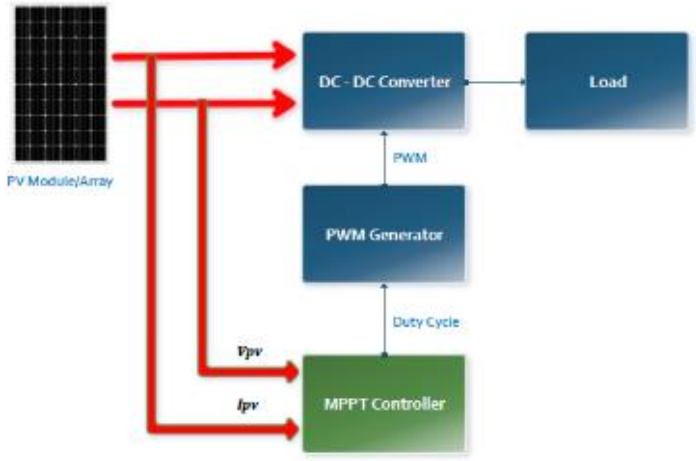

Fig. 3.2 Typical MPPT based PV system.

The duty cycle of the boost converter serves to regulate the load resistance experienced by the solar panel, effectively minimizing any mismatch between the two components. This ensures optimal power transfer between the source (solar panel) and the load. Please refer to Figure 3.3 for an illustration of a boost converter used as an adapter in this configuration [28].

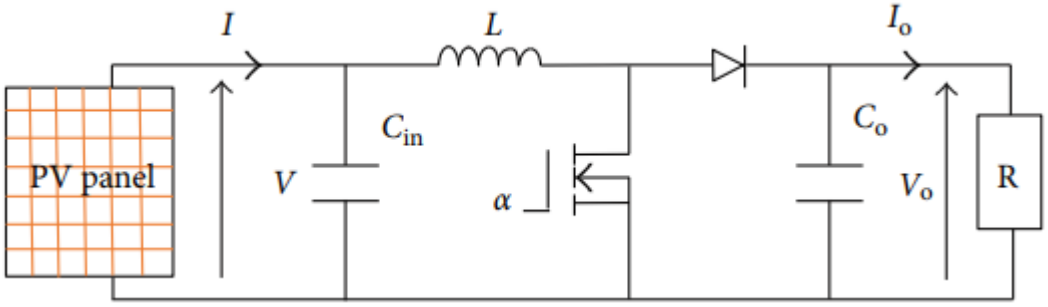

Fig. 3.3 Boost Converter in an MPPT based PV System.

3.4 Classification of Maximum Power Point Tracking Algorithms

The classification of **MPPT** algorithms can be based on the function of the techniques or control strategies used. Thus, two categories can be presented: direct methods and indirect methods.

3.4.1 Indirect methods

Indirect methods utilize databases that gather the characteristics of photovoltaic (**PV**) panels under different weather conditions (temperature, sunlight intensity, etc.), as well as empirical mathematical equations to determine the maximum power point.

These methods are often specific to each panel type and therefore difficult to generalize. Examples of indirect methods include curve fitting, look-up table, open-circuit voltage method, and short-circuit method.

- **Method based on open-circuit voltage measurement.**

This method is based on using a **PV** cell as a reference standard. This non-loaded reference cell is placed next to the **PV** modules and measures the real-time open-circuit voltage, which will determine the reference voltage.

To determine the operating point corresponding to the maximum power point in terms of voltage, a graph is plotted. This obtained function is nonlinear. To simplify the calculation, it needs to be linearized. These yields: [29]

$$V_{opt} = 0.7\, V_{oc} + 0.328 \qquad 3.1$$

With the **PV** voltage corresponding to the **MPP**.

Although the operating point is close to the maximum power, there are some criticisms of this method:

- Complete dependence on the reference cell, which can undergo modifications and anomalies.
- Failure to consider variations in the characteristics of PV modules.
- The voltage represents 75 to 95% of the voltage, so the linearization reduces accuracy.

- **The method based on short-circuit current.**

Measurement relies on calculating a reference current based on the short-circuit current using a proportional relationship given as follows [30].

$$I_{opt} = k\, I_{sc} \qquad 3.2$$

The current is periodically measured by performing short circuits of the **PV** array. This method, which requires only a single sensor, is easier to implement and slightly less expensive. However, it has the following disadvantages:

- In reality, the optimal current is between 85 to 95% of the short-circuit current, so it is not truly linear, resulting in a lack of precision.
- It does not take into account the **PV** array's characteristics due to external parameters.
- Energy loss occurs during the short-circuit time required for reference measurement.

3.4.2 Direct methods

Are methods that use voltage and current measurements from the panels, and their algorithm is based on the variation of these measurements. The advantage of these algorithms is that they do not require prior knowledge of the **PV** panel characteristics. Among these methods, we find the differentiation method, the Perturb and Observe (**P&O**) method, conductance incrementation, and others.

- **Perturbation and Observation algorithm P&O**

The principle of **P&O** type **MPPT** control is to perturb the **PV** voltage $\boldsymbol{V_{pv}}$ with a small amplitude around its initial value and analyse the resulting power variation $\boldsymbol{P_{pv}}$. From this analysis, it can be deduced that if a positive increment of $\boldsymbol{V_{pv}}$ leads to an increase in $\boldsymbol{P_{pv}}$, it means that the operating point is to the left of the **MPP**. Conversely, if the power decreases, it implies that the system has passed the **MPP**. A similar reasoning can be applied when the voltage decreases. By analysing the consequences of voltage variation on the $\boldsymbol{P_{pv}}$ ($\boldsymbol{V_{pv}}$) characteristic, it is easy to determine the operating point relative to the **MPP** and converge towards the maximum power through an appropriate control strategy. In summary, if, following a voltage perturbation, the **PV**

power increases, adjustments are made to further increase the voltage. If the **PV** power decreases, adjustments are made to decrease the voltage.

In summary, if following a voltage perturbation, the **PV** power increases, the perturbation direction is maintained. Otherwise, it is reversed to resume convergence towards the new **MPP** [31].

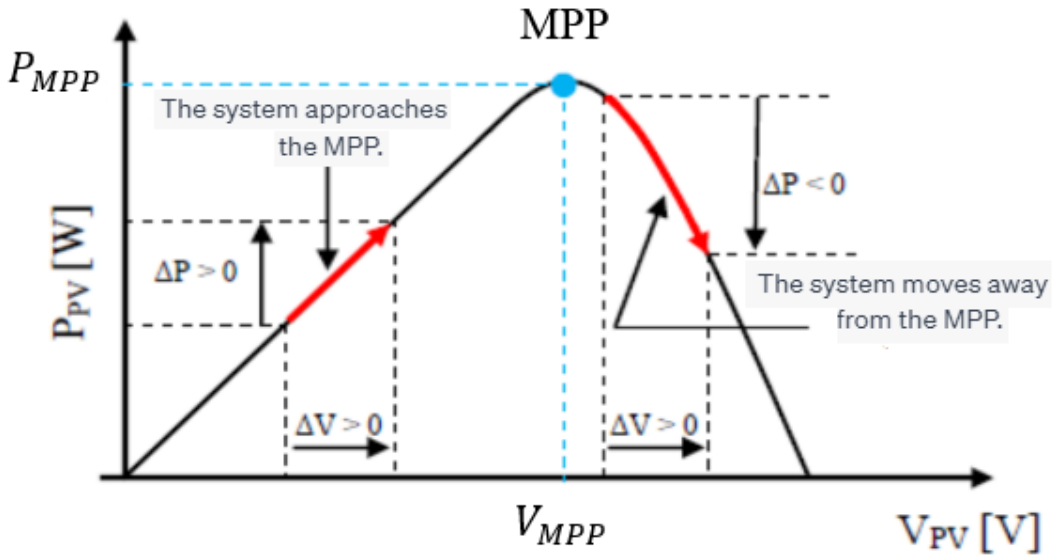

Fig. 3.4 I-V characteristic curve of a solar panel.

	ΔV	ΔP	$\frac{\Delta P}{\Delta V}$	Direction of tracking	Control action
1	+	+	+	Good	Increase $V_{ref} = V_{ref} + \Delta V$
2	-	-	+	Bad	Increase $V_{ref} = V_{ref} + \Delta V$
3	+	-	-	Bad	Decrease $V_{ref} = V_{ref} - \Delta V$
4	-	+	-	Good	Decrease $V_{ref} = V_{ref} - \Delta V$

Table. 3.1 Principle of the P&O algorithm.

The **P&O** algorithm (Figure 3.5) has the advantage of accuracy and quick response. It allows determining the maximum power point for a given sunlight intensity, temperature, or level of degradation of characteristics. However, the problem with this algorithm is:

- The oscillation around the MPP under normal operating conditions.
- The poor convergence of the algorithm in cases of sudden variations in temperature and/or sunlight intensity.

It should be noted that these oscillations can be reduced by using a small step size, but at the expense of convergence time. Therefore, a compromise must be made between precision and speed when choosing the update step size.

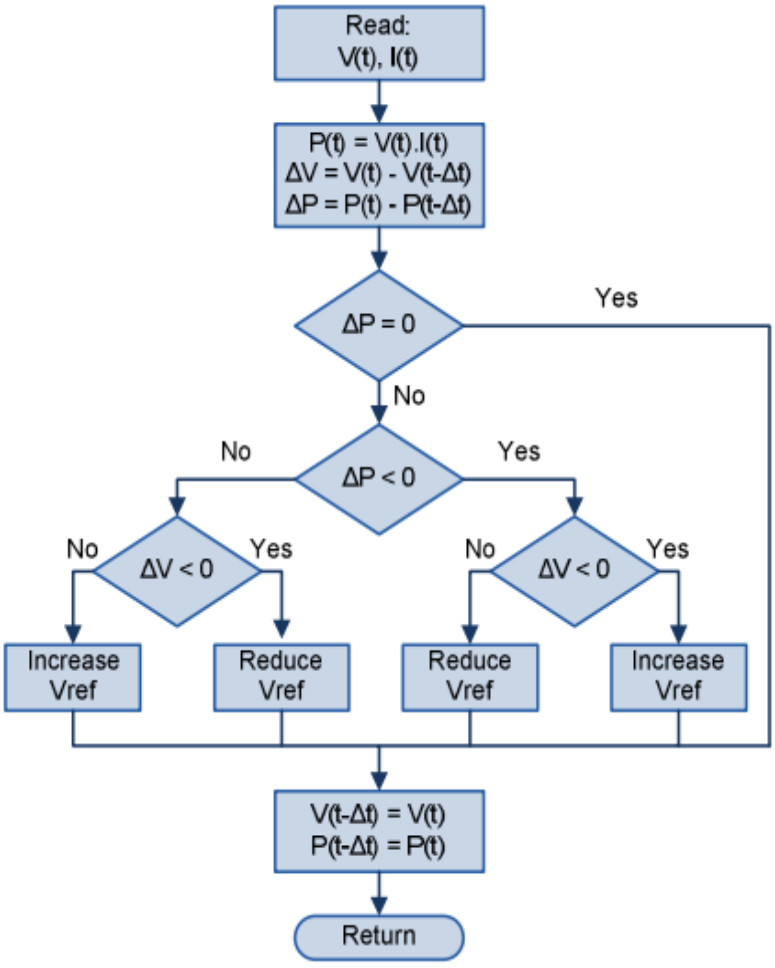

Fig. 3.5 Flowchart of the P&O method. [32]

- **Hill Climbing Algorithm**

The Hill Climbing (**HC**) technique [33, 34] is a mathematical optimization method. As the name suggests, it climbs along a characteristic curve to reach the maximum power point of the **PV** generator with respect to the duty cycle of the converter α (Figure 3.6). Perturbation is applied for several iterations on the parameter $\boldsymbol{\alpha}$ by incrementing or decrementing it.

By decrementing $\Delta\boldsymbol{\alpha}$ until the derivative $\boldsymbol{dP/d\alpha}$ becomes zero. Figure 3.7 illustrates the execution algorithm of this technique. The **HC** method is simpler to implement as it has only one control loop. However, it exhibits oscillations and can even diverge when there are rapid changes in atmospheric conditions.

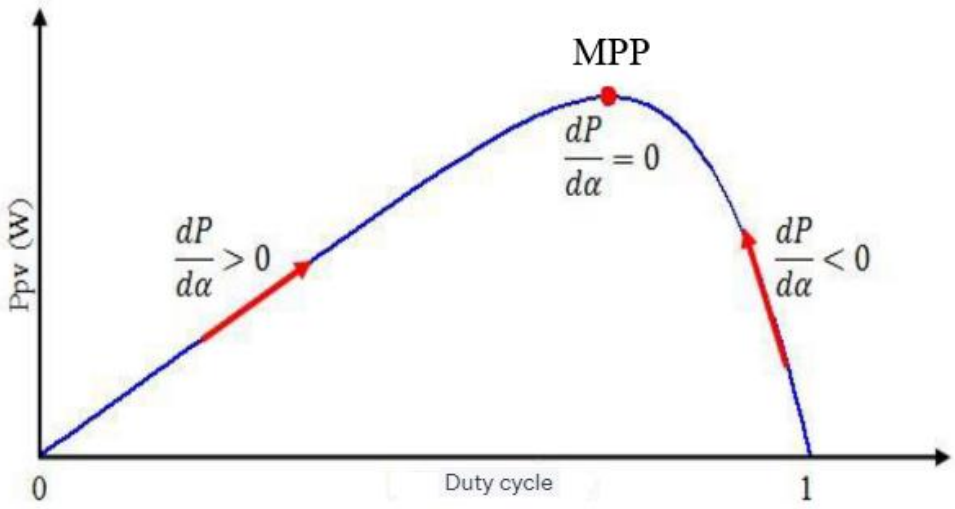

Fig. 3.6 Principle of the Hill Climbing method.

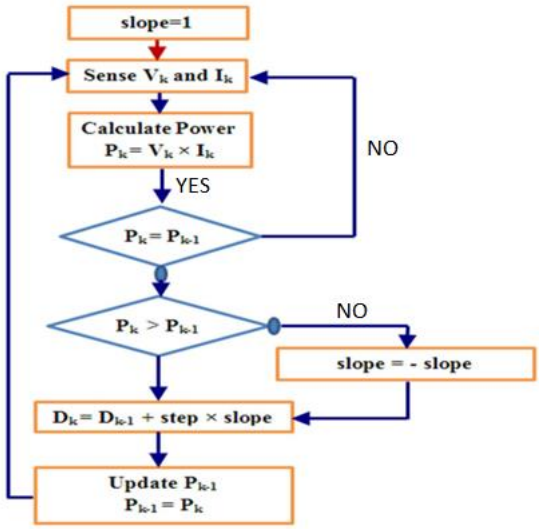

Fig. 3.7 Algorithm of the Hill Climbing method. [35]

- **Incremental Conductance Algorithm**

The Incremental Conductance algorithm, also known as "IncCond" in the literature, is another technique within the Hill Climbing (**HC**) family, where the **MPPT** controller attempts to move the operating point (**OP**) of the **PV** system along the **P-V** characteristic curve to reach the **MPP**. It achieves this by searching for the **MPP** based on the equality of conductance ($\boldsymbol{G = I/V}$) and the incremental conductance ($\boldsymbol{\Delta G = \Delta I/\Delta V}$) (see Figure 3.8). This algorithm requires knowledge of the initial value of the **OP** (Vref) and the voltage reference update step size (Δ**V**) (Figure 3.9).

The maximum power is obtained when the derivative of the **PV** system's power with respect to voltage becomes zero:

$$\frac{dP}{dV} = V\,\frac{dI}{dV} + I \cong V\,\frac{\Delta I}{\Delta V} + I \qquad 3.3$$

By comparing the conductance and the incremental conductance, three positions of the operating point (OP) can be distinguished:

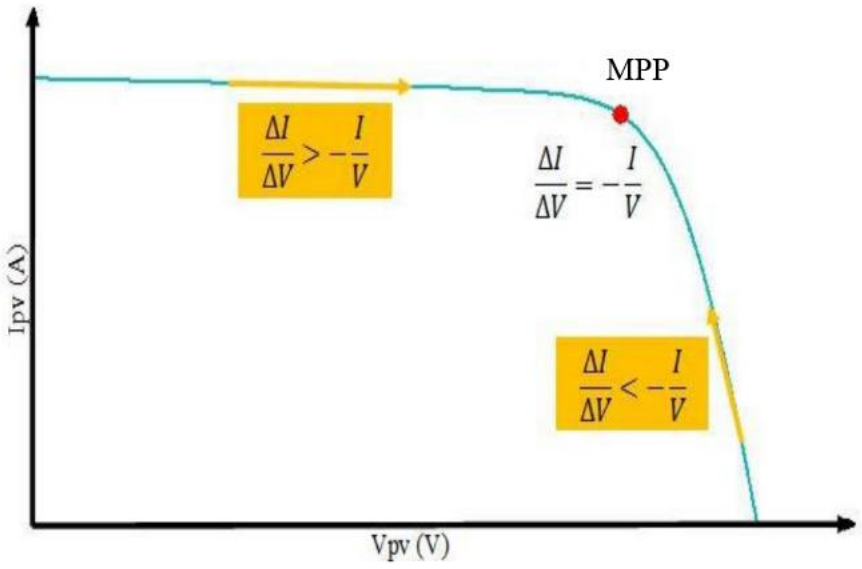

Fig. 3.8 Operating characteristic of the IC method.

The advantage of this algorithm is its precision and speed in searching for the **MPP** when atmospheric conditions change rapidly. This can be a remedy for the issues encountered with the **P&O** algorithm [36]. However, implementing this algorithm can be challenging due to the complexity of the control circuit, and real-time calculation of the derivative requires a fast-computing processor [36]. In other words, executing the **IC** control requires more time compared to **P&O**. In practical terms, even **IC** exhibits oscillations around the **MPP**. A comparison of the **MPPT** efficiency between the two most used techniques, **P&O** and **IC**, is presented in reference [37]. The results show an efficiency of 89.9% for **IC** compared to 81.5% for **P&O**.

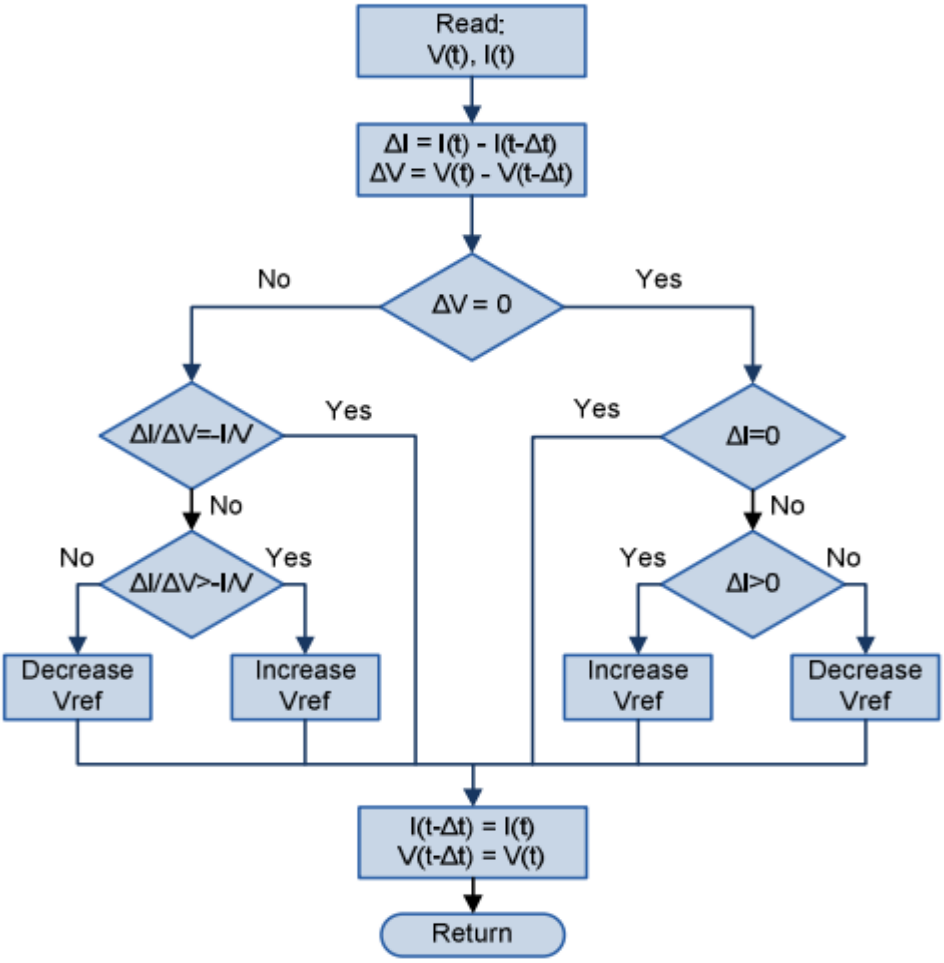

Fig. 3.9 Flowchart of the IC method.

3.5 Conclusion

In this chapter, we have also explored **MPPT** algorithms in detail. There are many ways to classify and group techniques for tracking the **MPP** of a **PV** generator. However, in this chapter, we focused on direct and indirect techniques.

In the next chapter, we will focus on soft computing algorithms and Novel Techniques.

Chapter 4: Soft Computing Algorithms and Novel Techniques

4.1 Introduction

Metaheuristic algorithms are optimization techniques inspired by natural processes or social behaviors. They are used to solve complex and difficult optimization problems where there is no exact algorithmic solution or where classical methods are ineffective. Metaheuristics employ principles such as local search, global search, cooperation, evolution, swarm behavior, and more, to explore the solution space and find a high-quality approximate solution. These algorithms offer high flexibility and robustness, making them well-suited for many real-world problems that require in-depth optimization approaches.

Due to the limitations observed in the conventional techniques discussed earlier, especially their inability to effectively handle partial shading conditions, various soft computing and artificial intelligence algorithms have been proposed to address these issues and enhance the tracking performance in both dynamic and steady-state scenarios. Many of these alternative approaches make use of metaheuristic algorithms, which have demonstrated excellent performance regardless of the operating conditions.

In this chapter we will study particle swarm optimization (**PSO**), grey wolf optimization (**GWO**), Seagull Optimizer algorithm and the Guided Seagull Optimizer.

4.2 Particle Swarm Optimization

4.2.1 Inspiration

Particle Swarm Optimization (**PSO**) is inspired by the behaviour of insect swarms, particularly birds in flight or schools of fish. These swarms exhibit interesting collective properties, such as the ability to quickly find food sources or avoid obstacles, through coordination and communication among individuals. These observations have inspired the development of the Particle Swarm Optimization algorithm, where each "particle" represents a potential solution in the search space. The particles move and explore the solution space based on their own experience and information shared with their neighbours. This enables efficient exploration of both local and global optima, leading to high-quality solutions for optimization problems.

The algorithm has been developed by Dr. Eberhart and Dr. Kennedy in 1995. [38]

4.2.2 Principle of working

Particle Swarm Optimization (**PSO**) is a population-based stochastic search method inspired by the behaviour of bird flocks. The **PSO** algorithm maintains a swarm of individuals known as particles, where each particle represents a candidate solution. The particles follow a simple behaviour: they mimic the success of their neighbouring particles and their own success [39].

The position of a particle is influenced by the best particle in its neighbourhood, called $\boldsymbol{P_{best}}$ as well as the best solution found by all particles in the entire population, known as $\boldsymbol{g_{best}}$ The position of the particle, $\boldsymbol{x_i}$ is adjusted using the following formula:

$$x_i^{t+1} = x_i^t + v_i^{t+1} \qquad 4.1$$

The velocity component, $\boldsymbol{v_i}$ represents the magnitude of the step or displacement for each particle. The velocity is calculated using the following formula:

$$v_i^{t+1} = w\, v_i^t + c_1 r_1 \,(P_{best}\,, i - x_i^t\,) + c_2 r_2 \,(g_{best} - x_i^t\,) \qquad 4.2$$

With $i = 1, 2, \ldots\ldots N$.

Where:

N: Number of particles

Where $\boldsymbol{x_i}$ denotes the position of the particle for **i**, the velocity of the particle at **i** is represented by $\boldsymbol{v_i}$; the number of iterations is denoted by **t**; the inertia weight is represented by **ω**; $\boldsymbol{r_1}$ and $\boldsymbol{r_2}$ are uniformly distributed random variables in **[0, 1]**; and the cognitive and social coefficients are denoted as $\boldsymbol{c_1}$ and $\boldsymbol{c_2}$, respectively. The best position found so far for particle **i** is represented by the variable $\boldsymbol{P_{best}}$, and the best position among all particles is represented by $\boldsymbol{g_{best}}$. Figure 4.1 illustrates the particle movement in the optimization process [39].

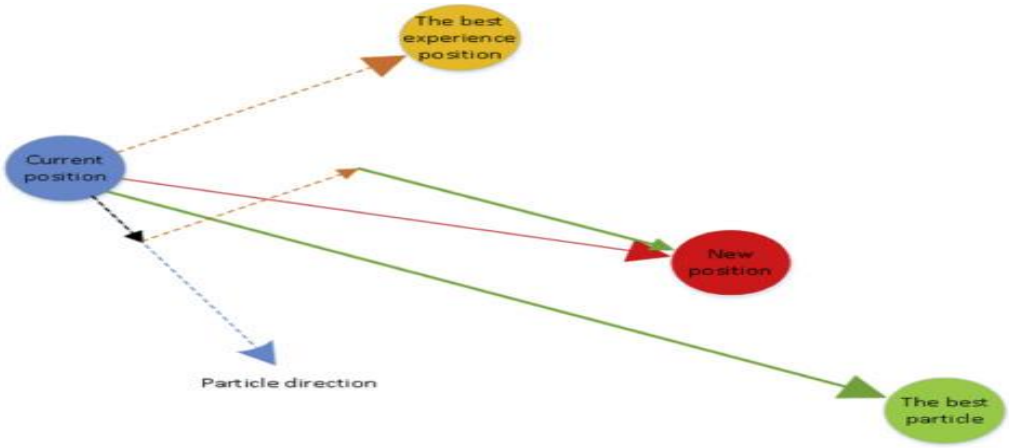

Fig. 4.1 Particle movement in the optimization process. [40]

Conventional **PSO** is fast and accurate in searching for the output characteristic curves of **PV** modules with simple peak values. However, conventional **PSO**-based **MPPT** needs to be modified when some modules in a **PV** array are shaded.

4.2.3 Key Features

This model has some interesting properties that make it a useful tool for many optimization problems, particularly highly nonlinear, continuous, or mixed problems (where some variables are real, and others are integers):

- It is easy to program, requiring just a few lines of code in any advanced language.
- It is robust (poor parameter choices may degrade performance, but they do not prevent obtaining a solution).

4.2.4 Configuration of the Method

- **Number of Particles**

The number of particles allocated for solving the problem depends mainly on two parameters: the size of the search space and the ratio between the computational capabilities of the machine and the maximum search time. There is no specific rule for determining this parameter, and conducting multiple trials helps in gaining the necessary experience to grasp this parameter.

- **Neighbourhood Topology**

The neighbourhood defines the social network structure, where particles within a common neighbourhood communicate with each other. Different neighbourhood topologies have been studied (Kennedy, 1999) and are considered based on particle identifiers rather than topological information such as Euclidean distances in the search space:

- Star Topology (Figure 4.2.a): The social network is fully connected, where each particle is attracted to the best particle, denoted as g_{best}, and communicates with all others.

- Ring Topology (Figure 4.2.b): Each particle communicates with a fixed number (**n = 3**) of immediate neighbours. Each particle tends to move towards the best particle within its local neighbourhood, denoted as P_{best}.

- Radius Topology (Figure 4.2.c): In this topology, a "central" particle is connected to all the other particles. Only this central particle adjusts its position towards the best solution, and if it leads to an improvement, the information is propagated to the other particles.

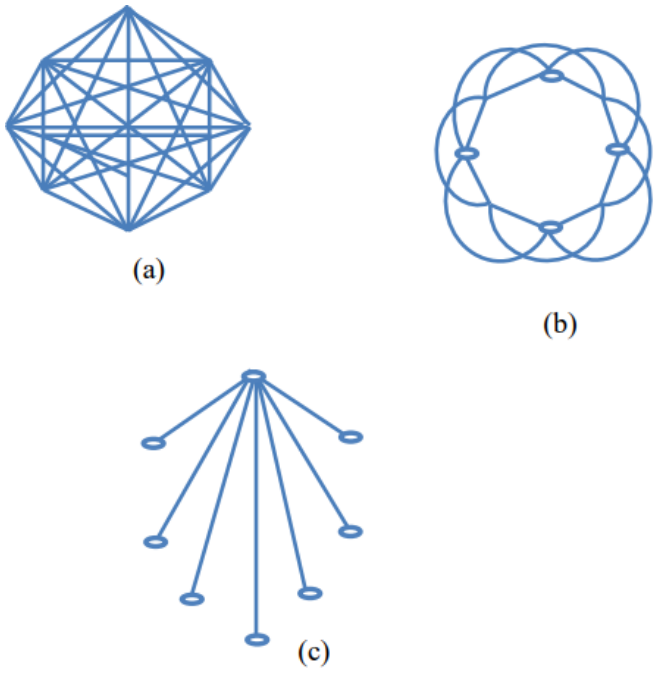

Fig. 4.2 Three different topologies: a) Star, b) Ring, c) Radial [41].

4.2.5 MPPT technique based on PSO (Particle Swarm Optimization)

For the **MPPT** system based on **PSO**, the particle's position is designated as the duty cycle of the power converter, while the fitness evaluation function has been chosen as the generated power P_{pv} for the entire photovoltaic system. In the proposed method overview, more accurate

MPP tracking is achieved despite complex environmental conditions with a smaller number of particles, whereas a larger number of particles would result in longer computation time. Therefore, it is important to strike a balance between tracking speed and accuracy [39].

During the initialization step of particle swarm optimization, particles can be randomly distributed within a range or placed in a stationary position. Generally, it makes more sense to initialize particles around the known position of the global maximum power point within the search range if such data is available. The authors indicate that the minimum displacement between successive peaks is approximately 80% of the open-circuit voltage ($\boldsymbol{V_{oc}}$), and the peaks on the **P-V** curve occur at nearly multiples of 80% of the module's open-circuit voltage ($\boldsymbol{V_{oc}}$). Thus, the number of particles **N** should be chosen accordingly.

The particle positions in the photovoltaic system are selected as random numbers. The search spaces of the particles, which cover [**0 1**], are initialized at a defined point. Here, **0** and **1** represent the minimum and maximum duty cycle values of the used **DC-DC** converter, respectively.

The objective of this **PSO**-based **MPPT** method is to extract the maximum power ($\boldsymbol{P_{pv}}$) from the photovoltaic system. To evaluate the fitness value, which is the generated power, the pulse width modulation (**PWM**) acts in line with the particle's position, indicating the duty cycle state. The photovoltaic voltage ($\boldsymbol{V_{pv}}$) and current ($\boldsymbol{I_{pv}}$) can be measured. These values can then be used to calculate the fitness value ($\boldsymbol{P_{pv}}$) of the particle. However, to obtain accurate samples, it should be noted that the power converter's stabilization time should be shorter than the evaluation time intervals between successive particles.

To address these issues, a linearly decreasing divergence with increasing iteration numbers has been adopted in this study for the **PSO** formula weighting. The physical meaning of this modified weighting formula is that larger step sizes are used to increase the particle search speed during the initial search when the distance to the global optimum is relatively large. This avoids excessively small step sizes that would lead to inevitable local optima traps. However, the step size gradually decreases as the number of iterations increases. As the particles approach the **MPP**,

the decrease in *w* reduces the particle's movement steps, allowing them to more accurately track the **MPP**.

In Equation (4.2), to maintain particle acceleration in the same direction it originally moved, the first term $\boldsymbol{\omega(t)Vi(t)}$ is used, which controls the convergence behavior of the particle swarm optimization. The inertia weight is chosen to accelerate convergence, such that the effect of **Vi(t)** diminishes over the algorithm process. The choice to decrease the value of **ω** over time is considered. To obtain refined solutions, a typical option is to initially set the inertia weight to a higher value and slowly reduce it for better exploration. For this reason, a linearly decreasing **ω** term is used, as illustrated below:

$$w(t) = w_{max} - \frac{t}{t_{max}} (w_{max} - w_{min}) \qquad 4.3$$

In equation (4.3), the minimum and maximum limits were denoted as $\boldsymbol{w_{min}}$ and $\boldsymbol{w_{max}}$, respectively, while the maximum allowed number of iterations was noted as tmax. Similarly, the social and cognitive terms can be reshaped. The optimization capability of particle swarms can be affected by the values of $\boldsymbol{c_1}$ and $\boldsymbol{c_2}$, which modify the direction of the particle. By selecting appropriate values for $\boldsymbol{c_1}$ and $\boldsymbol{c_2}$, the particles can strike a balance between exploring the search space and exploiting the best solutions found so far. These parameters play a crucial role in determining the convergence and performance of the **PSO** algorithm.

When $\boldsymbol{c_1} > \boldsymbol{c_2}$, the sampling with respect to the improvement of $\boldsymbol{P_{best}}$would be biased, while selecting $\boldsymbol{c_1} < \boldsymbol{c_2}$ would favour the sampling relative to the improvement of $\boldsymbol{g_{best}}$. For these reasons, these two terms are defined as continuously increasing and decreasing functions, as shown in equation (4.4) and (4.5) respectively:

$$c_1(t) = c_{1.max} - \frac{t}{t_{max}} (c_{1.max} - c_{1.min}) \qquad 4.4$$

$$c_2(t) = c_{2.max} - \frac{t}{t_{max}} (c_{2.max} - c_{2.min}) \quad 4.5$$

Two convergence criteria are used in this study. The proposed **MPPT** method based on **PSO** will stop and provide the best solution if the maximum number of iterations is reached or if all particle velocities become lower than a threshold. Generally, particle swarm optimization algorithms are used to solve optimization problems where the optimal result is time-invariant. However, in this case, the fitness value, which is the global maximum power point, sometimes varies or depends on environmental factors and charging states. To search for the new global **MPP** in such cases, the particles need to be reset. Considering the need to detect changes in solar radiation, the following constraint is used. In the proposed **PSO**-based technique, the particles will be reset whenever the following condition is met:

$$\frac{|P_{PVnew} - P_{PVold}|}{P_{PVold}} \geq \Delta P\ \% \quad 4.6$$

Where $\boldsymbol{P_{PVnew}}$ is the new photovoltaic power, $\boldsymbol{P_{PVold}}$ is the photovoltaic power at the previous global maximum operating point, and $\boldsymbol{\Delta P\ (\%)}$ is defined as 3%. [39]

The Figure 4.3 represents the complete flowchart of the **MPPT** technique algorithm based on **PSO**.

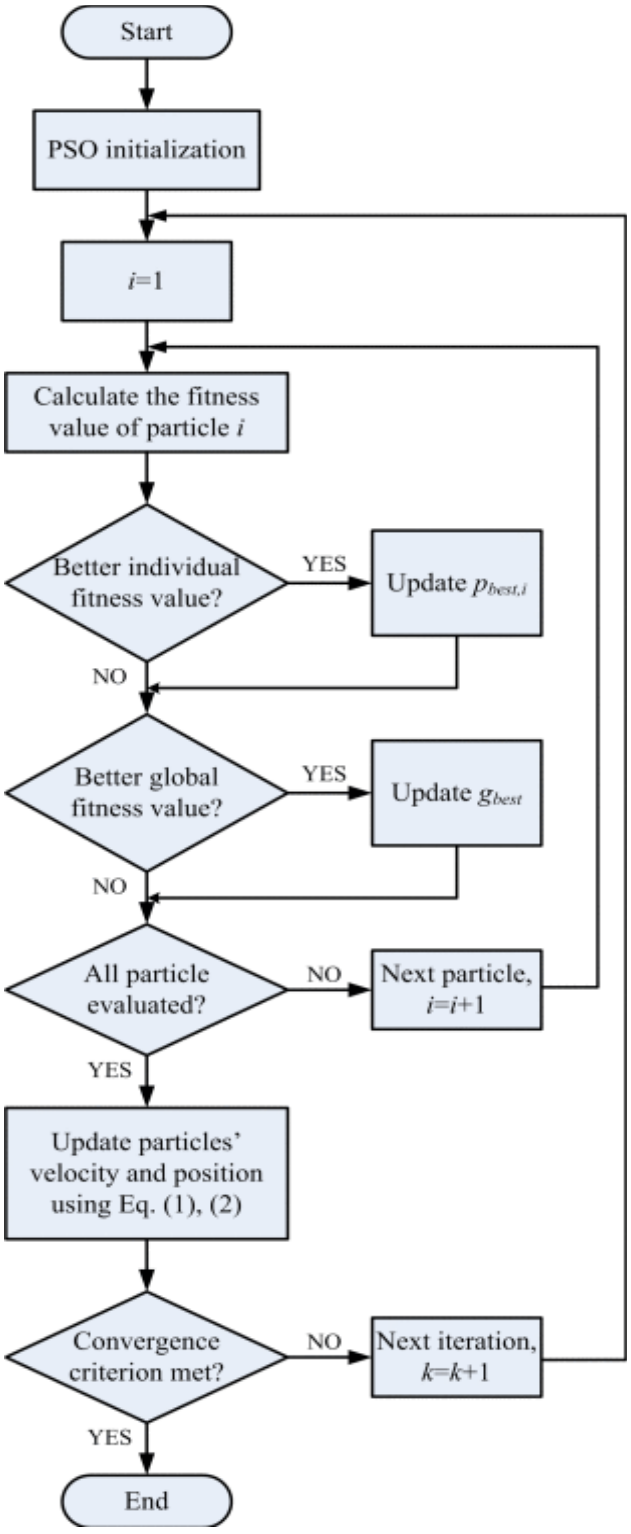

Fig. 4.3 Flowchart of the proposed MPPT algorithm based on PSO. [39].

The algorithm of this method can be described as follows:

Step 1: Initialize the coefficients $\boldsymbol{c_1}$ and $\boldsymbol{c_2}$, and the inertia coefficient **w**.

Step 2: Create the initial population randomly and calculate the fitness of each particle ($\boldsymbol{P_{best}}$): the best position of particle **i** in the current population; ($\boldsymbol{P_{gbest}}$): the best position among all populations (the best of the best).

Step 3: Calculate the new velocity and new position for each particle using formulas (4.5) and (4.6).

Step 4: Calculate the best fitness of the current population and compare it with the previous best to find the overall best position ($\boldsymbol{P_{gbest}}$).

Step 5: Increment the iteration count **t = t+1**.

Step 6: If a termination criterion is satisfied, go to **Step 7**. Otherwise, go to **Step 3**.

Step 7: The position saved in ($\boldsymbol{P_{gbest}}$) is the optimal solution [41].

```
Random generation of the initial population.
Calculate the fitness function.
Repeat
   Calculate the best fitness of the current population.
   Calculate the best fitness among all populations.
   Calculate the velocity of each particle.
   Calculate the position of each particle.
   Calculate the fitness function.
Until the termination criterion is satisfied
```

Fig.4.4 The pseudo-code for the proposed MPPT algorithm based on PSO.

4.2 Grey Wolf Optimization (GWO)

4.3.1 Introduction

This study proposes a new metaheuristic called Grey Wolf Optimizer (**GWO**) inspired by grey wolves (Canis lupus). The **GWO** algorithm mimics the leadership hierarchy and hunting mechanism of grey wolves in nature. Four types of grey wolves, namely alpha, beta, delta, and omega, are used to simulate the leadership hierarchy. Additionally, the three main steps of hunting, which include prey searching, prey encircling, and prey attacking, are implemented. The algorithm is then compared to 29 well-known test functions, and the results are verified through a comparative study with Particle Swarm Optimization (**PSO**), Gravitational Search Algorithm (**GSA**), Differential Evolution (**DE**), Evolutionary Programming (**EP**), and Evolution Strategy (**ES**). The results demonstrate that the **GWO** algorithm is capable of providing highly competitive results compared to these well-known metaheuristics.

4.3.2 Method of Grey Wolf Optimization (GWO)

The **GWO** method is a new algorithm proposed by Iranian researcher Mirjalili in 2014 [42]. The GWO algorithm utilizes the simulation of social authority represented by the victim encircling behaviour to obtain the optimal solution to the optimization problem. This algorithm mimics the hierarchical dominance technique of grey wolves during the hunting operation for the victim until their movements stop. **GWO** is similar to population-based algorithms in the search for a solution by simulating the natural behaviour of grey wolves in their social life when they search for food.

The first level represents the pack leader called "alpha," the second level in the hierarchy is called "beta," which assists alpha in decision-making. The next level includes delta and omega, which are the lowest ranks and eat last after the wolves from other levels. In fact, the wolves are group hunters who go through three main steps: searching, encircling, and attacking.

The algorithm starts with a given number of grey wolves with their positions generated randomly.

4.3.3 Inspiration

The grey wolf, a type of wolf, is part of the Canidae family. Grey wolves are powerful predators and are known as the kings of their food chain. They usually live together in groups called packs, which consist of about 5 to 12 wolves on average. One interesting aspect of their behaviour is their strict social order, as illustrated in Figure 4.5.

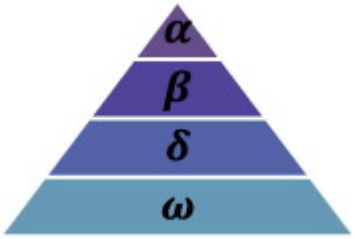

Fig. 4.5 Hierarchy of the grey wolf (dominance decreases from top to bottom).

The grey wolf pack has a well-defined social structure with leaders called alphas, consisting of a male and a female. The alpha makes important decisions for the pack, such as hunting strategies, sleeping locations, and wake-up times. The pack members follow the alpha's decisions, but they also exhibit democratic behaviour by following other wolves. The alpha is recognized by the pack during gatherings when they lower their tails.

The alpha wolf, also known as the dominant wolf, has the authority to mate within the pack. However, being the alpha is not based on physical strength but on leadership skills and management abilities. The second rank in the hierarchy is the beta, who assists the alpha in decision-making and enforcing discipline within the pack. Betas can be male or female and are potential successors to the alpha position.

The lowest rank is the omega, serving as the scapegoat and submitting to all dominant wolves. Omegas are the last to eat but play a crucial role in maintaining pack harmony. They help release tension and maintain the dominance structure within the pack. Subordinates, also known as deltas, have various roles such as scouts, sentinels, elders, hunters, and caretakers. Scouts monitor the territory, sentinels protect the pack, elders provide experience, hunters assist with hunting, and caretakers care for the weak and injured.

In addition to the social hierarchy, grey wolves exhibit fascinating group hunting behaviour. The hunting process involves specific phases, as described by Muro et al. [43].

- Tracking, pursuing, and approaching the prey.
- Chasing, encircling, and harassing the prey until it stops moving.
- Attacking the prey.

These stages are illustrated in Figure 4.6.

Fig. 4.6 Gray Wolf Hunting Behaviour: (A) Hunting, Tracking, and Approaching Prey (B-D) Pursuing, Harassing, and Encircling (A) Stalking and Attacking [42].

In this work, the hunting behaviour and social hierarchy of grey wolves are mathematically modelled to design GWO and perform optimization.

4.3.4 Mathematical Model and Algorithm

In this subsection, mathematical models for social hierarchy, tracking, encircling, and attacking prey are formulated. Then, the GWO algorithm is described.

- **Social Hierarchy**

To mathematically model the social hierarchy of wolves in the design of **GWO**, we consider the most suitable solution as alpha (**α**). Therefore, the second and third best solutions are named beta (**β**) and delta (**δ**) respectively. The remaining candidate solutions are assumed to be omega (**ω**). In the **GWO** algorithm, hunting (optimization) is guided by **α**, **β**, and **δ**. The wolves follow these three leaders.

- **Encircling Prey**

As mentioned above, grey wolves encircle their prey during hunting. To mathematically model the encircling behaviour, the following equations are proposed:

$$D = \left| C\, X_p(t) - X(t) \right| \tag{4.7}$$

$$X(t+1) = \left| X_p(t) - A\, D \right| \tag{4.8}$$

Where **t** denotes the current iteration, **A** and **C** are coefficient vectors, $\boldsymbol{X_p}$ represents the position vector of the prey, and **X** indicates the position vector of a gray wolf. The vectors **A** and **C** are calculated as follows:

$$\alpha = 2\left(\frac{1-t}{T_{max}}\right) \quad 4.9$$

$$A = 2\,a\,r_1 - a \quad 4.10$$

$$C = 2\,r_2 \quad 4.11$$

Grey wolves live in groups called packs, and within these packs, there is a clear social order. The pack is led by an alpha male and an alpha female, who make important decisions for the group, such as where to hunt and when to sleep. The rest of the pack follows their lead. Sometimes, the alpha wolf will also follow the others in the pack, showing a democratic behaviour.

The alpha wolf is the most dominant and is in charge of mating within the pack. Interestingly, being the alpha is not about being the strongest, but rather being the best at managing the pack. The second-ranking wolf in the hierarchy is called the beta, who assists the alpha in making decisions and keeping order within the pack. The lowest-ranking wolf is the omega, who submits to all other wolves in the pack and often serves as a target for their frustration and aggression.

Other wolves in the pack are called subordinates or deltas. They have specific roles, such as scouting the territory, protecting the pack, providing experience, helping with hunting, and taking care of the weak and injured members.

Group hunting is another important behaviour of grey wolves. It involves different phases and requires coordination among the pack members.

Overall, grey wolves have a complex social structure with leaders, followers, and various roles within the pack.

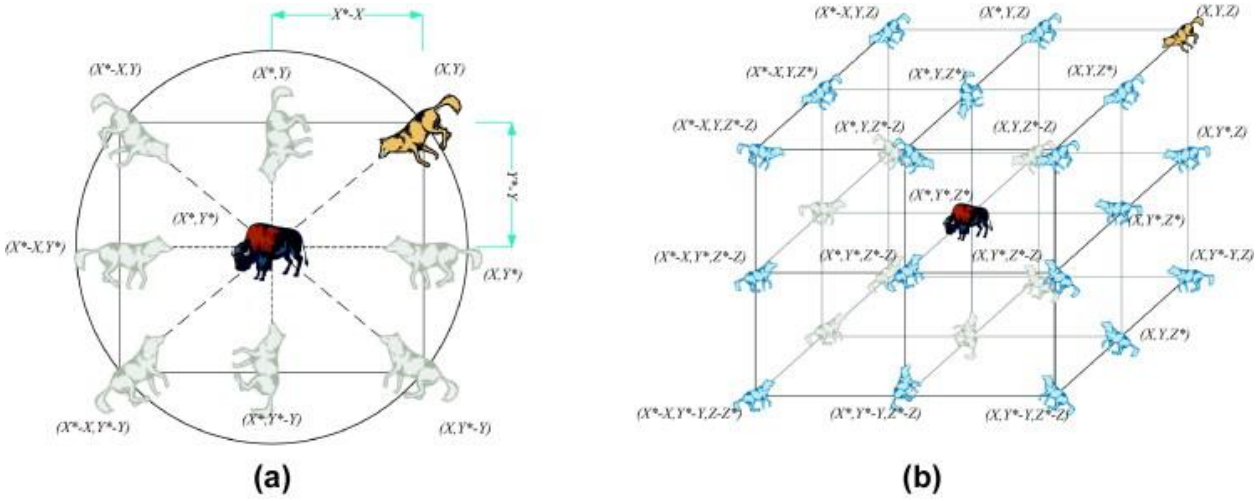

Fig. 4.7 2D and 3D Position Vectors and Their Possible Next Locations.

- **Hunting**

Grey wolves have the ability to track and encircle their prey. When hunting, they are usually guided by the alpha wolf. The beta and delta wolves may also join in the hunt occasionally. However, when it comes to searching for prey in an unknown space, we have no idea about the exact location of the optimal prey. To mathematically model the hunting behaviour of grey wolves, we make the assumption that the alpha (the best candidate solution), beta, and delta have a better understanding of where the prey might be. Therefore, we keep track of the three best solutions found so far and instruct other search agents, including the omega wolves, to update their positions based on the position of the best search agent. The following formulas are proposed to accomplish this

$$\begin{aligned} D_\alpha &= |C_1\, X_\alpha(t) - X(t)| \\ D_\beta &= |C_2\, X_\beta(t) - X(t)| \\ D_\delta &= |C_3\, X_\delta(t) - X(t)| \end{aligned} \qquad 4.12$$

$$X_1 = X_\alpha - A_1 D_\alpha X_2$$
$$X_2 = X_\beta - A_2 D_\beta X_3 \qquad 4.13$$
$$X_3 = X_\delta - A_3 D_\delta$$

$$X(t+1) = \frac{(X_1 + X_2 + X_3)}{3} \qquad 4.14$$

In Figure 4.8, you can see how a search agent changes its position based on the positions of alpha, beta, and delta in a 2D search area. The final position of the agent ends up in a random spot inside a circle formed by the positions of alpha, beta, and delta. This means that alpha, beta, and delta give an idea of where the prey might be, and the other wolves adjust their positions randomly around the prey.

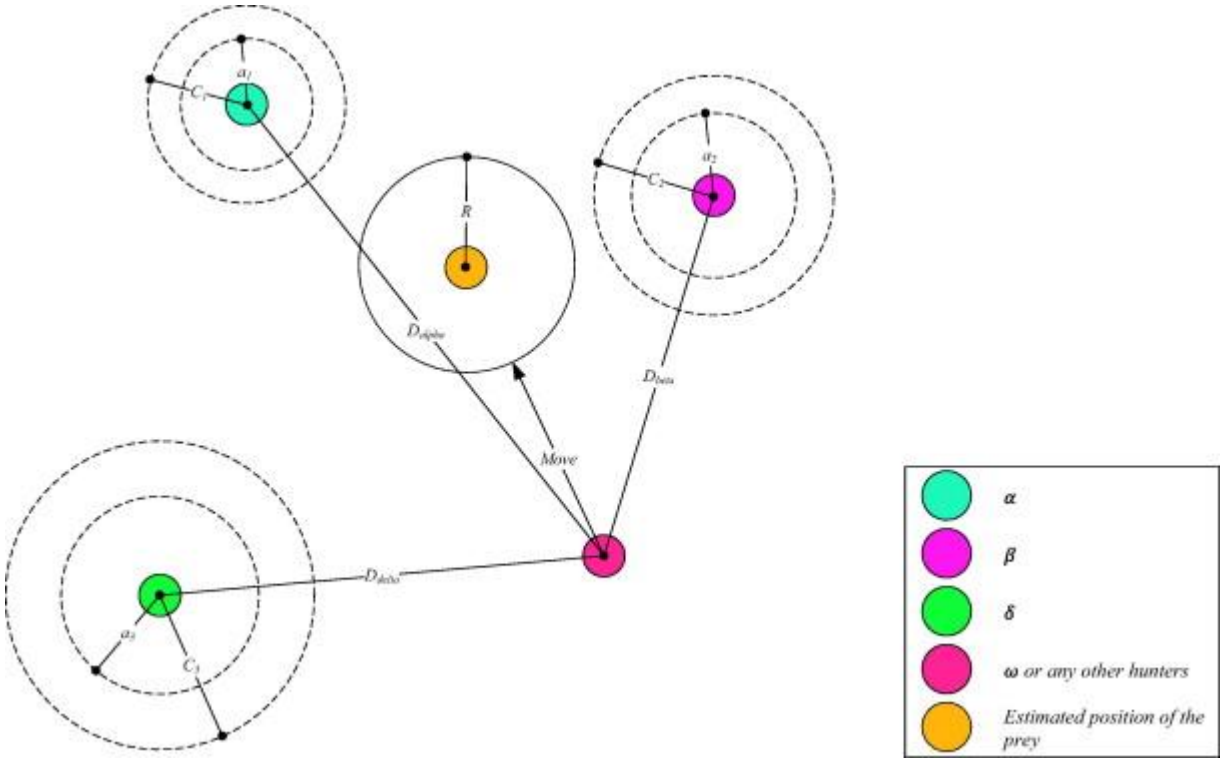

Fig. 4.8 Updating the position in GWO.

- **Attacking a prey (exploitation)**

As mentioned earlier, grey wolves end their hunt by attacking the prey when it stops moving. To mathematically represent this approach, we reduce the value of **|A|**. It's important to note that the range of possible values for **|A|** also decreases as **|A|** decreases from 2 to 0 over time. In simpler terms, **|A|** randomly takes values within the interval **[-a,a],** where a decreases from **2** to **0** during each iteration. When the random values of |A| fall within the range **[-1,1],** the next position of a search agent can be anywhere between its current position and the position of the prey. Figure 4.9.a illustrates that when **|A|** is less than **1**, the wolves are compelled to attack towards the prey.

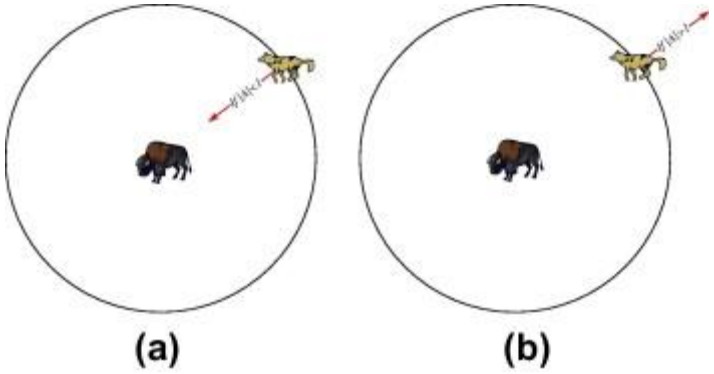

Fig. 4.9 Attacking a prey or searching for a prey.

Using the operators suggested up until now, the **GWO** algorithm enables its search agents to adjust their position by considering the positions of the alpha, beta, and delta, and to target the prey. However, these operators make the **GWO** algorithm prone to getting stuck in local solutions without further exploration. Although the encircling mechanism proposed provides some level of exploration, the **GWO** algorithm needs additional operators that focus more on exploration.

- **Searching for prey (exploration)**

Gray wolves in the **GWO** algorithm search based on the positions of alpha, beta, and delta. They diverge and converge to find and attack prey. The algorithm uses random values to control their movement. The **C** component promotes exploration by adding randomness to the distance calculation. The search starts with a random population of wolves, and they update their positions based on the prey's estimated location. The algorithm emphasizes both exploration and exploitation. It terminates when a final criterion is met.

The algorithm starts by initializing a population of grey wolves, labelled as $\boldsymbol{X_i}$, $\boldsymbol{i} = 1,2..N$ It also initializes the variables **a**, **A**, and **C**. The fitness of each search agent is then calculated. $\boldsymbol{X_\alpha}$ represents the best search agent, $\boldsymbol{X_\beta}$ represents the second-best search agent, and $\boldsymbol{X_\delta}$ represents the third best search agent.

The algorithm then enters a loop that continues until a maximum number of iterations is reached. Within each iteration, the position of each search agent is updated using equation (4.14). After updating the positions, the variables **a**, **A**, and **C** are updated. The fitness of all search agents is recalculated, and the values of $\boldsymbol{X_\alpha}$, $\boldsymbol{X_\beta}$, and $\boldsymbol{X_\delta}$ are updated accordingly.

The iteration count, **t**, is incremented, and the loop continues until the maximum number of iterations is reached.

Initialize the grey wolf population $\boldsymbol{X_i}$ **(i = 1, 2, ..., n)**.

Initialize **a, A**, and **C**.

Calculate the fitness of each search agent.

$\boldsymbol{X_\alpha}$is assigned to the best search agent.

$\boldsymbol{X_\beta}$ is assigned to the second best search agent.

$\boldsymbol{X_\delta}$ is assigned to the third best search agent.

While t is less than the maximum number of iterations:

For each search agent:

    Update the position of the current search agent using equation (4.14).

End for.

Update **a**, **A**, and **C**.

Calculate the fitness of all search agents.

Update $\boldsymbol{X_\alpha}$, $\boldsymbol{X_\beta}$, and $\boldsymbol{X_\delta}$.

Increment **t** by **1**.

End while.

Return $\boldsymbol{X_\alpha}$

Fig. 4.10 The pseudo code for the Grey Wolf Optimization (GWO).

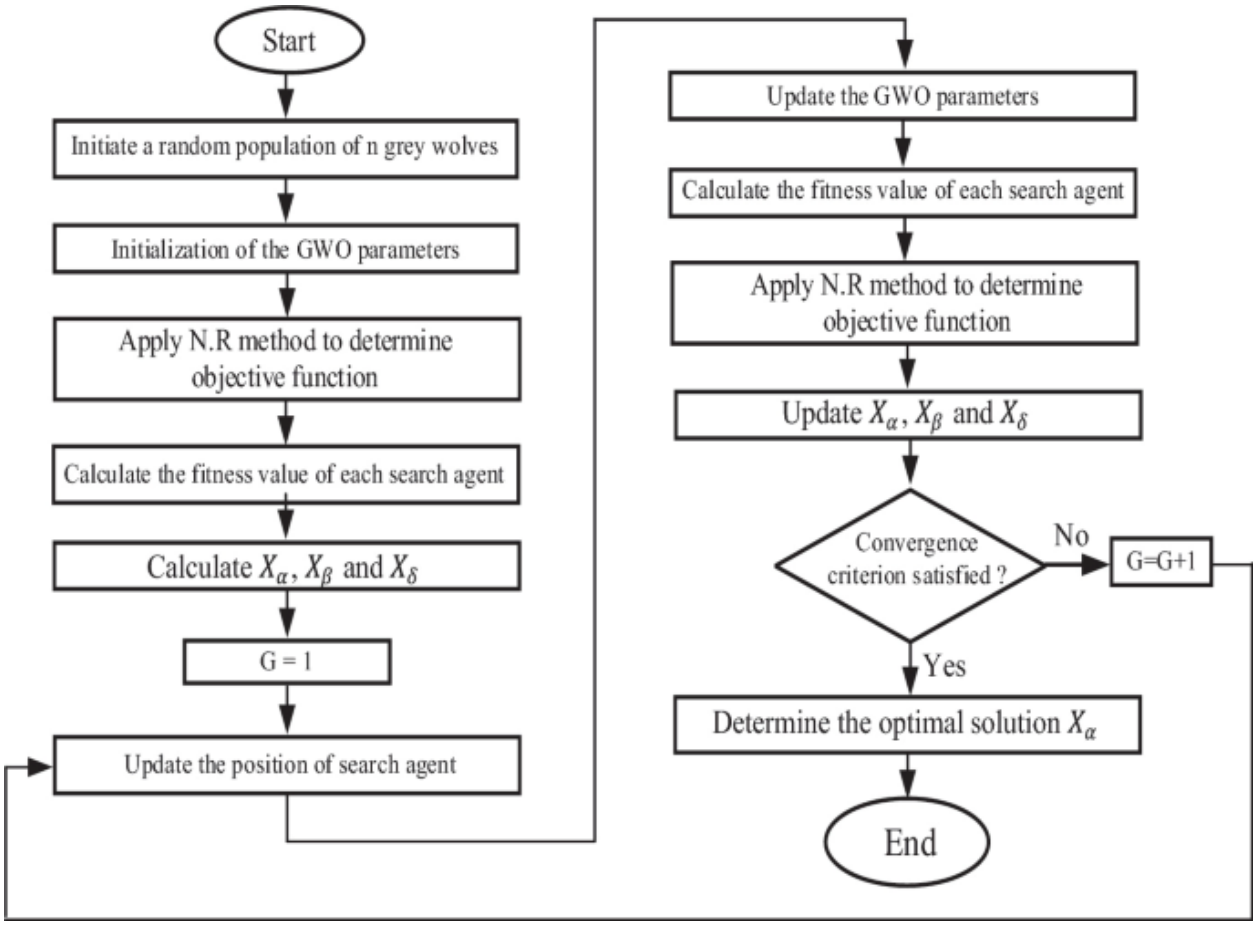

Fig. 4.11 The flowchart of GWO algorithm.

4.3 Seagull Optimization Algorithm

4.4.1 Inspiration:

The Seagull Optimization algorithm is a novel bio-inspired technique for solving computationally expensive problems. The main inspiration of this algorithm is the migration and attacking strategies of a family of clever birds known as seagulls. They learn, remember and even pass on behaviours, such as stamping their feet in a group to imitate rainfall and trick earthworms to come to the surface. They even have a complex and highly developed repertoire for communication which includes a range of vocalizations and body movements [48].

Generally, seagulls live in colonies. They use their intelligence to find and attack the prey. The most important thing about seagulls is their migrating and attacking mechanisms. The following represents the key behaviours used by the Seagull Optimization technique [49].

• During migration, they travel in a group. The initial positions of seagulls are different to avoid the collisions between each other.

• In a group, seagulls can travel towards the direction of best survival fittest seagull.

• Based on the fittest seagull, other seagulls can update their initial positions.

• Seagulls frequently attack migrating birds over the sea [50] when they migrate from one place to another. They can make their spiral natural shape movement during attacking. A conceptual model of these behaviours is illustrated in Figure 4.12.

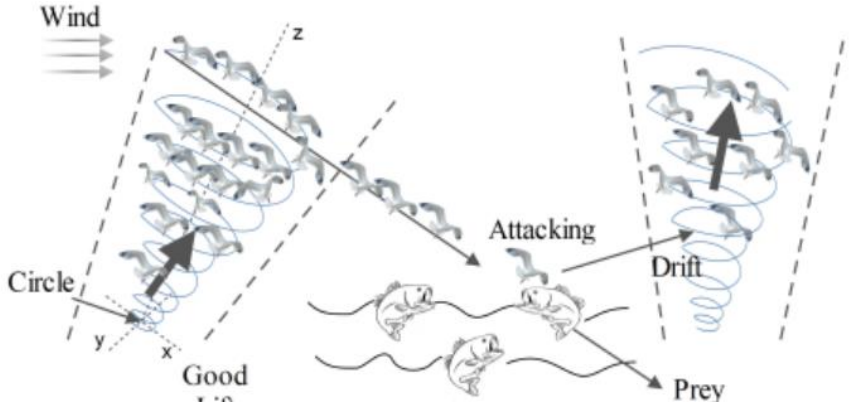

Fig. 4.12 Migration and Attacking Behaviours of Seagulls. [50]

4.4.2 SOA Modelling and process steps:

4.4.2.1 Migration:

This stage is served as the exploration phase. The algorithm here simulates how a group of seagulls moves from one location to another. The bird should satisfy the following three conditions:

- **Avoiding Collisions**: A variable is employed to calculate the new search agent position as follows:

$$\vec{C}_S = A \times \vec{P}_S(t) \quad 4.15$$

Where $\vec{C}_S$ represents the position of the search agent that does not collide with other individuals. $\vec{P}_S(t)$ is the search agent current position at iteration **t**, and **A** represents the movement behaviour of the individual, and it is decreased linearly over the optimization process as follows:

$$A = f_c - f_c \times \frac{t}{T} \quad 4.16$$

Where f_c is a control parameter that depends on the optimization problem.

- **Movement towards best neighbour's direction**:

After avoiding collisions between neighbours, the search agents are moved towards the direction of the best location as follows:

$$\vec{M}_s = B \times \left(\vec{P}_{bs}(t) - \vec{P}_s(t)\right) \quad 4.17$$

Where $\vec{M}_s$ is the individual's position towards the best search agent location, **B** is given in equation 4.18 and it is responsible for proper balancing between exploration and exploitation:

$$B = 2 \times A^2 \times rnd \quad 4.18$$

Where **rnd** is random number within the range [0,1].

- **Remain close to the best search agent**:

Lastly, the search agents will update their positions with respect to the best location using equation 4.19:

$$\vec{D}_S = \left|\vec{C}_S + \vec{M}_S\right| \qquad 4.19$$

4.4.2.2 Attacking:

The attacking process is served as the exploitation phase. Here a spiral equation is employed to mimic the helix-shaped movement of seagulls while hunting and entrapping the prey. This behaviour is depicted in figure 4.13 and it is modelled in x, y and z planes as follows:

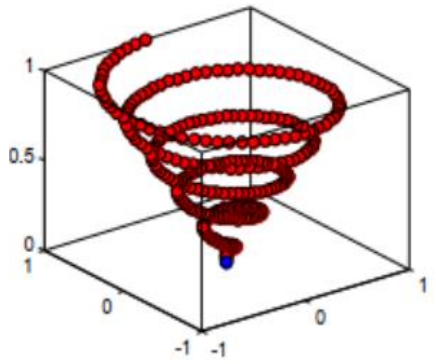

Fig. 4.13 Natural Attacking behaviour of Seagulls.

$$x = r \times \cos\cos(k)$$
$$y = r \times \sin\sin(k) \qquad 4.20$$
$$z = r \times k$$
$$r = u \times e^{kv}$$

Where:

- **r** represents the radius of each turn of the spiral.
- **k** is a random number in the range [0, 2π].
- $\boldsymbol{u}$ and $\boldsymbol{v}$ are constants to define the spiral shape.

The search agents' positions are then updated using equation 4.21, which represents the general framework of the Seagull Optimization algorithm:

$$\overrightarrow{P_s} = \left(\overrightarrow{D_s} \times x \times y \times z\right) + \overrightarrow{P_{bs}} \qquad 4.21$$

4.4.3 SOA based MPPT:

The flowchart illustrating the SOA based MPP tracker is depicted in figure 4.14.

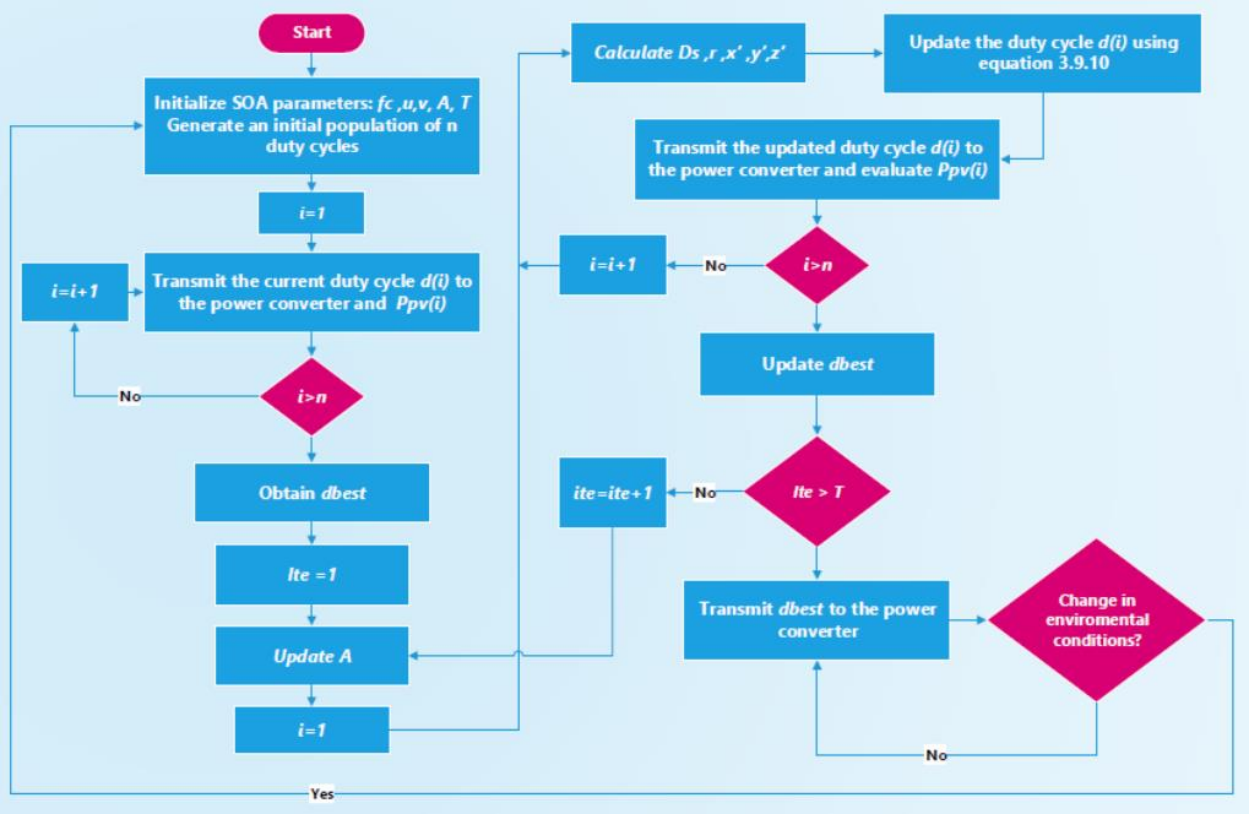

Fig. 4.14 SOA based MPPT Algorithm.

4.4 Guided Seagull Optimizer

Although the standard SOA proved to be efficient in dealing with a decent range of applications, its standard equation might cause local optimum stagnation. This is mainly because it relies on the global best solution over the whole iterative process. For that matter, opposition learning for the global best solution is incorporated over half the iterations with half the population as follows:

if $t < \frac{T}{2}$

if $i \leq \frac{N}{2}$

$$\overrightarrow{X_{t+1}(l)} = \left(\overrightarrow{D_s(l)} \times x'(i) \times y'(i) \times z'(i)\right) + \overrightarrow{X_B}$$

else

$$\overrightarrow{X_{t+1}(l)} = \left(\overrightarrow{D_s(l)} \times x'(i) \times y'(i) \times z'(i)\right) + \overrightarrow{X_{BO}} \quad 4.22$$

end if

else

$$\overrightarrow{X_{t+1}(l)} = \left(\overrightarrow{D_s(l)} \times x'(i) \times y'(i) \times z'(i)\right) + \overrightarrow{X_B} \quad 4.23$$

end if

Where $\overrightarrow{X_{BO}}$ is computed using the next equation:

$$\overrightarrow{X_{BO}} = \overrightarrow{UB} + \overrightarrow{LB} - \overrightarrow{X_{BO}} \quad 4.24$$

Moreover, it is always desirable to reduce perturbations in the operating point while tracking the Maximum power point in order to minimize Power losses. In light of that, the controlling factor A is modified in such a way that it maintains adequate jumps during the first half of the iterations, and produces tiny movements during the second half.. The modifications are as follows :

if $t < \frac{T}{2}$

$$A = 1 - 1 \times \frac{t}{T} \quad (4.25)$$

else

$$A = 0.5 - 0.5 \times \frac{t}{T} \quad (4.26)$$

end if

The overall operating flowchart of the GSO algorithm is depicted in Fig 4.15.

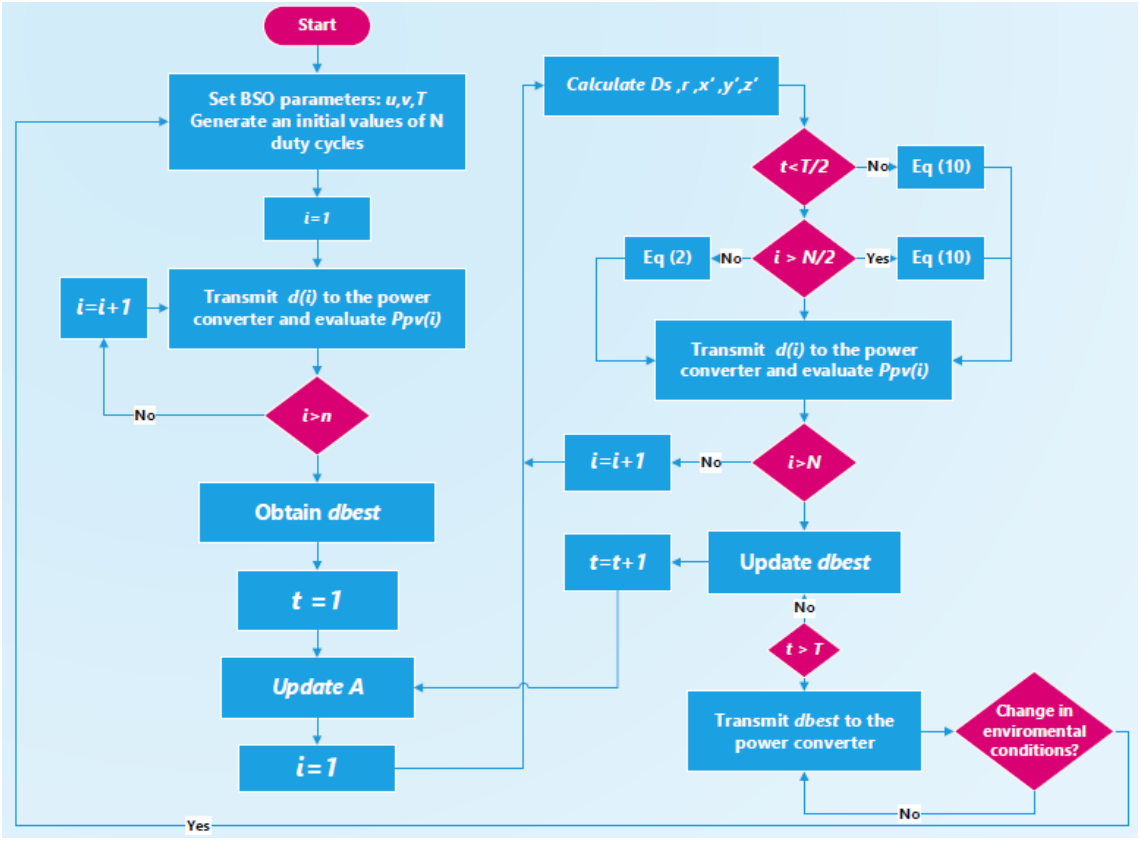

Fig. 4.15 GSO Operating Flowchart for MPPT.

4.5 Conclusion

This chapter set forth four well-known nature inspired algorithms, as well as the latest developments in the field of metaheuristics. A survey that consists of the inspiration and mathematical modelling of these optimizers, and their operating flowcharts in maximum power tracking, was provided. In the next chapter, we are going to evaluate the propound techniques in an MPPT based standalone PV system.

CHAPTER 5: SIMULATION AND RESULTS

5.1 Introduction:

To assess the effectiveness of the proposed techniques, MATLAB and Simulink are used to simulate a simple stand-alone system subjected to several atmospheric conditions. A comparative study in terms of robustness, tracking speed and efficiency is provided at the end of this chapter.

5.2 System Overview:

The Simulink model of our system is illustrated in figure 5.1 It consist of 7 panels of the same type, a boost converter driven by an MPPT controller, and a load of 40Ω.

5.3 DC-DC boost converter design:

Setting the switching frequency to 50 KHz, the components of the power converter are selected as shown in the next table:

Switching Frequency	Inductor (L)	Input Capacitor	Output Capacitor
50 KHz	$5 \times e^{-3}$ H	$5 \times e^{-5}$ F	$1 \times e^{-10}$ F

Table 5.1. Boost Converter Components.

It is worth mentioning that in order to get accurate measurements of the output PV power that corresponds to each duty cycle, the time interval between two successive transmissions of D should be greater than the boost converter settling time. To do so, several values of the duty cycle have to be tested to analyse the transient response of the power converter and the time it takes to settle down. After performing this evaluation, we have found that a sampling time of 0.008s is appropriate for our system.

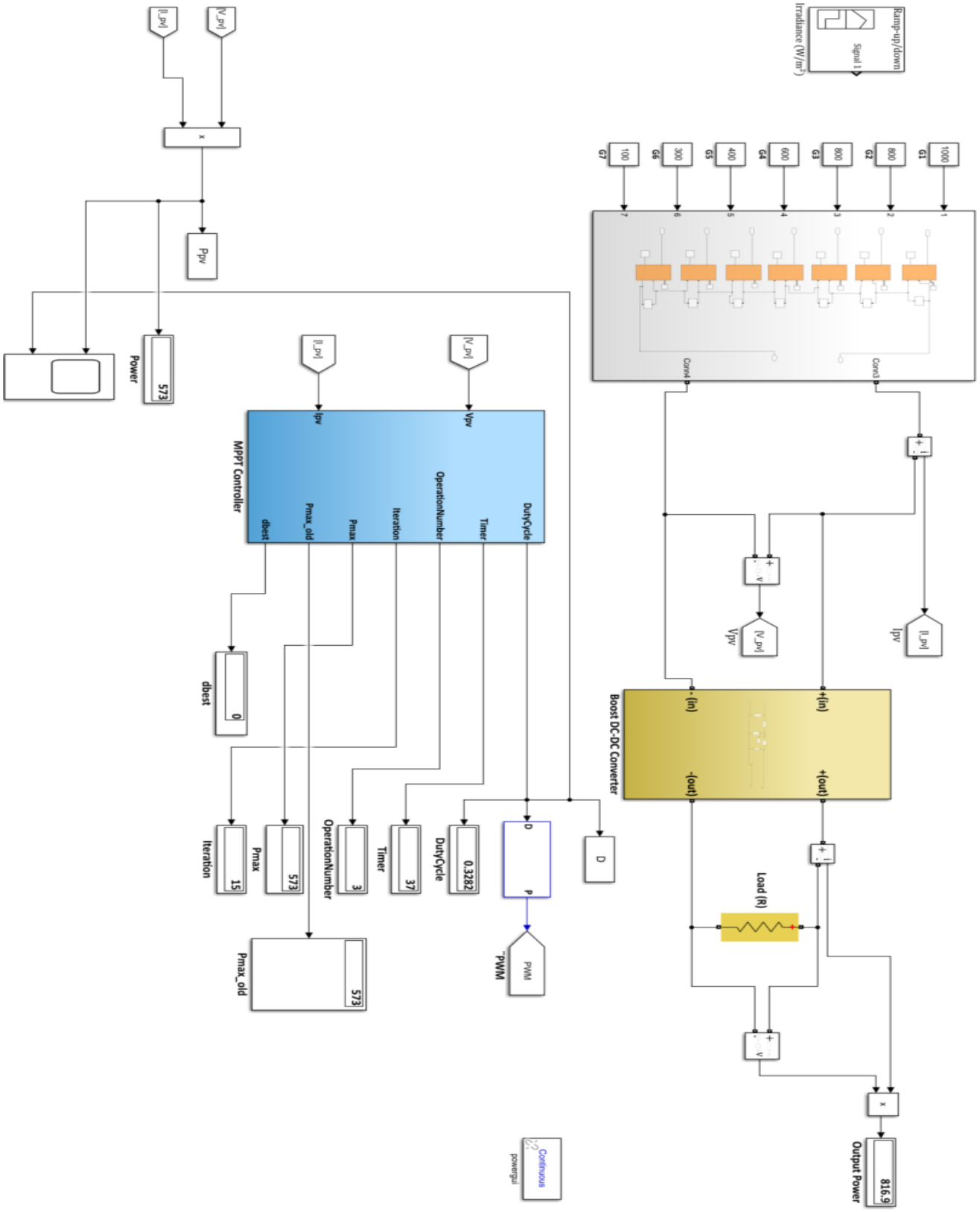

Fig 5.1 Simulink Model of the designed System.

5.4 Algorithms Parameterization:

Table 5.2 provides the selected parameters of every optimizer; the reader should notice that the settings may differ to that provided in the original papers of these algorithms which might be unsuitable for MPPT applications.

The selection of the population size N has a significant impact on the performance of the optimizer. A large N will improve the search ability and tracking accuracy; however, this will increase the convergence time of the algorithm. On the other hand, a small N speeds up the search process, but it may lead to poor power efficiency.

In this work, and in order to make a fair comparison, we have selected N to be 4, which seems to be a reasonable choice. The maximum number of iterations is set to 10 for all algorithms.

Algorithms	Parametrization
PSO	$\omega = 0.9\text{-}0.8t/T$ $c_1 = 1.2 \quad c_2 = 2$
GWO	$a = 0.7 - 0.7t/T$
SOA	$A = 0.7 - 0.7t/T$ $u = 0.8, v = 0.05$
GSO	$u = 0.8, v = 0.05$

Table 5.2. Algorithms Parameterization.

5.5 Results and Discussion:

Six distinct scenarios have been subjected to the PV system. In the first case, the PV array receives a fast-varying uniform irradiance that changes every 0.5 seconds in three different levels: 500-1000-750 W/m². In the five remaining cases, different partial shading patterns with various

numbers of peaks have been exposed to the substrings that constitute our PV modules. Table 5.3 and figure 5.3 illustrate the different scenarios and their PV characteristics.

Cases	Irradiance levels distribution on the modules Substrings (W/m^2)	GMPP (W)
1-Uniform Fast Varying Irradiance	[0s,0.5s]:500 [0.5s,1s]:1000 [1s,1.5s]:750	755.94 $1.49\ e+03$ $1.13\ e+03$
2-PSC	300/300/800/800/600/600/300	546.27
3-PSC	1000/1000/600/300/300/800/600	703.69
4-PSC	1000/400/800/800/300/600/600	699.75
5-PSC	1000/500/800/700/300/600/500	709.13
6-PSC	1000/500/800/700/900/600/400	733.94

Table 5.3. Irradiance levels of the uniform fast varying and the partial shading condition.

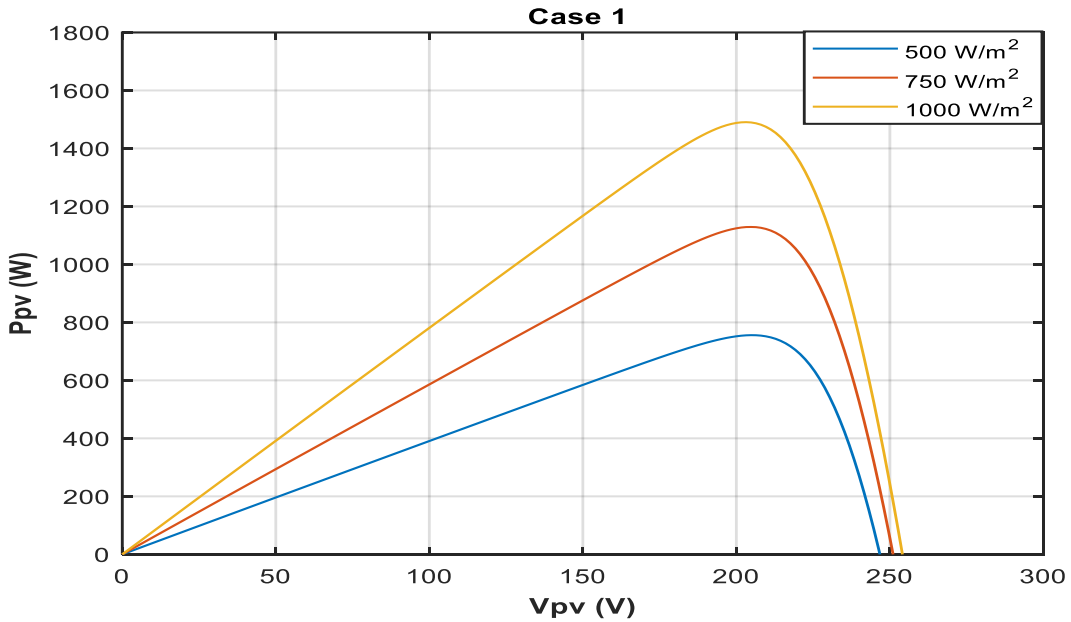

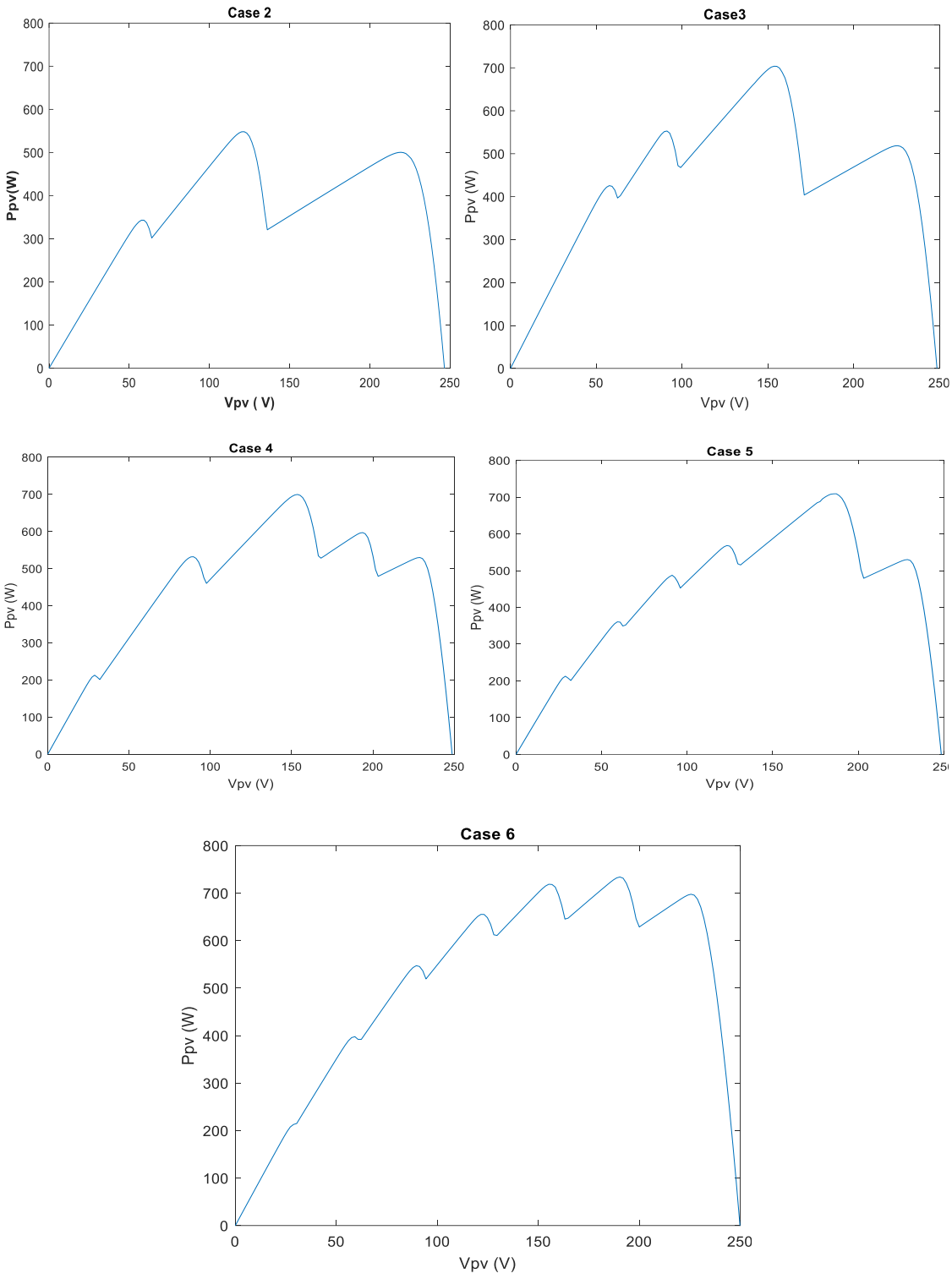

Fig 5.2 P-V curves of the considered Partial Shading Conditions.

5.5.1 Uniform Fast Varying irradiance.

The resulting PV power curves for each algorithm with uniform fast varying irradiation are shown in figure 5.3 where all algorithms were able to detect changes in irradiation levels and locate the maximum power point. Table 5.4 provides the results details of the simulation in terms of efficiency and time convergence in each time interval.

Optimizer	GMPP(W)	Tracked Power (W)	Convergence Time (s)
PSO	755.94	551.1 - **1491** - 1128	**0.07** – 0.26 – 0.1
GWO	1.49 $e+03$	549 – **1491**- X	**0.22** - 0.32 - X
SOA	1.13 $e+03$	551 – **1490** – 1128	**0.06** – 0.25 – 0.11
GSO		551 – **1491** - 1126	**0.16** - 0.2 – 0.2

Table 5.4. Simulation of the fast-varying irradiation.

In order to have a better assessment measure, we consider the average efficiencies and average convergence time as provided in the next table.

Optimizer	Average Efficiency	Average Convergence Time
PSO	90.94	0.143
GWO	86.31	0.27
SOA	90.91	0.140
GSO	90.87	0.18

Table 5.5. Average efficiency and convergence time of the fast-varying irradiation.

It can be observed that all algorithms have nearly equal efficiencies, but with a considerable difference in convergence time. With SOA, PSO and GSO being fastest respectively.

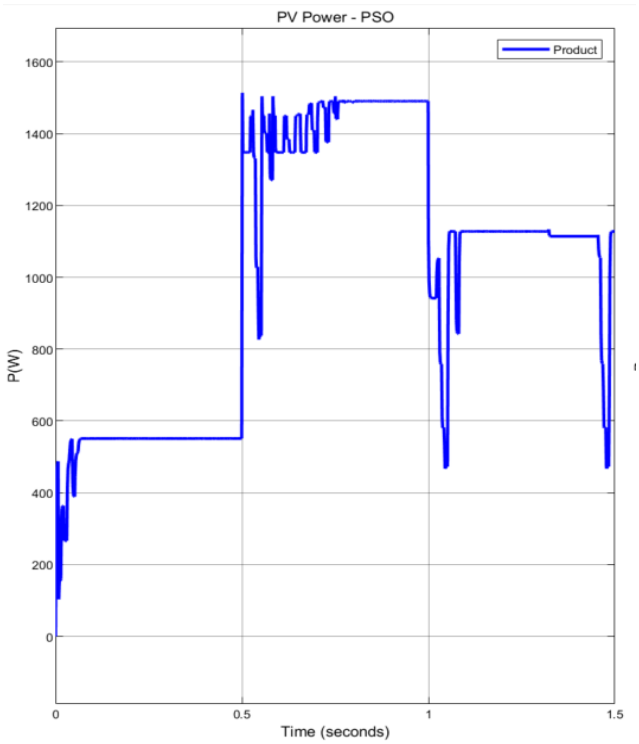
PV Power - PSO
Product
P(W)
Time (seconds)
0
200
400
600
800
1000
1200
1400
1600
0
0.5
1
1.5

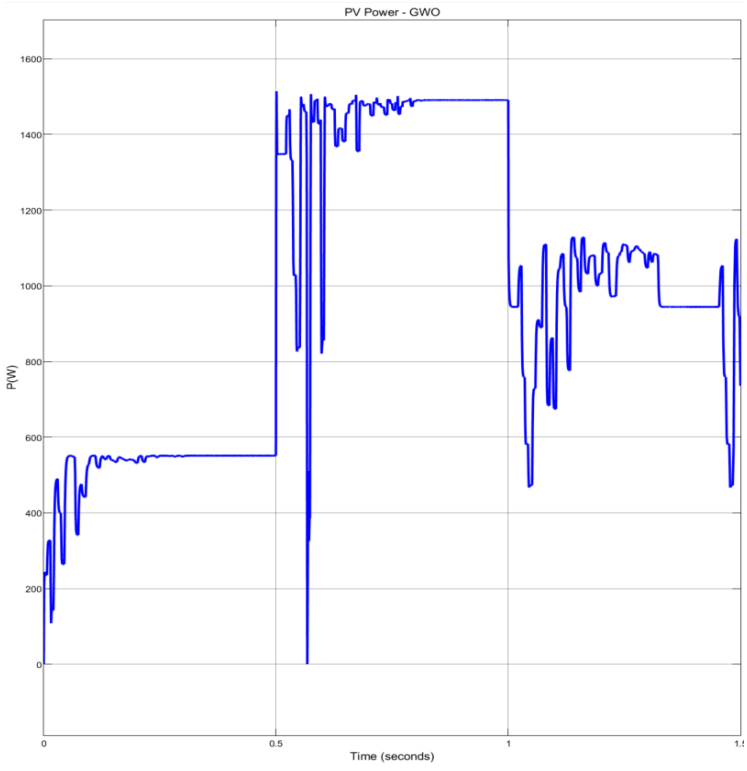
PV Power - GWO
P(W)
Time (seconds)
0
200
400
600
800
1000
1200
1400
1600
0
0.5
1

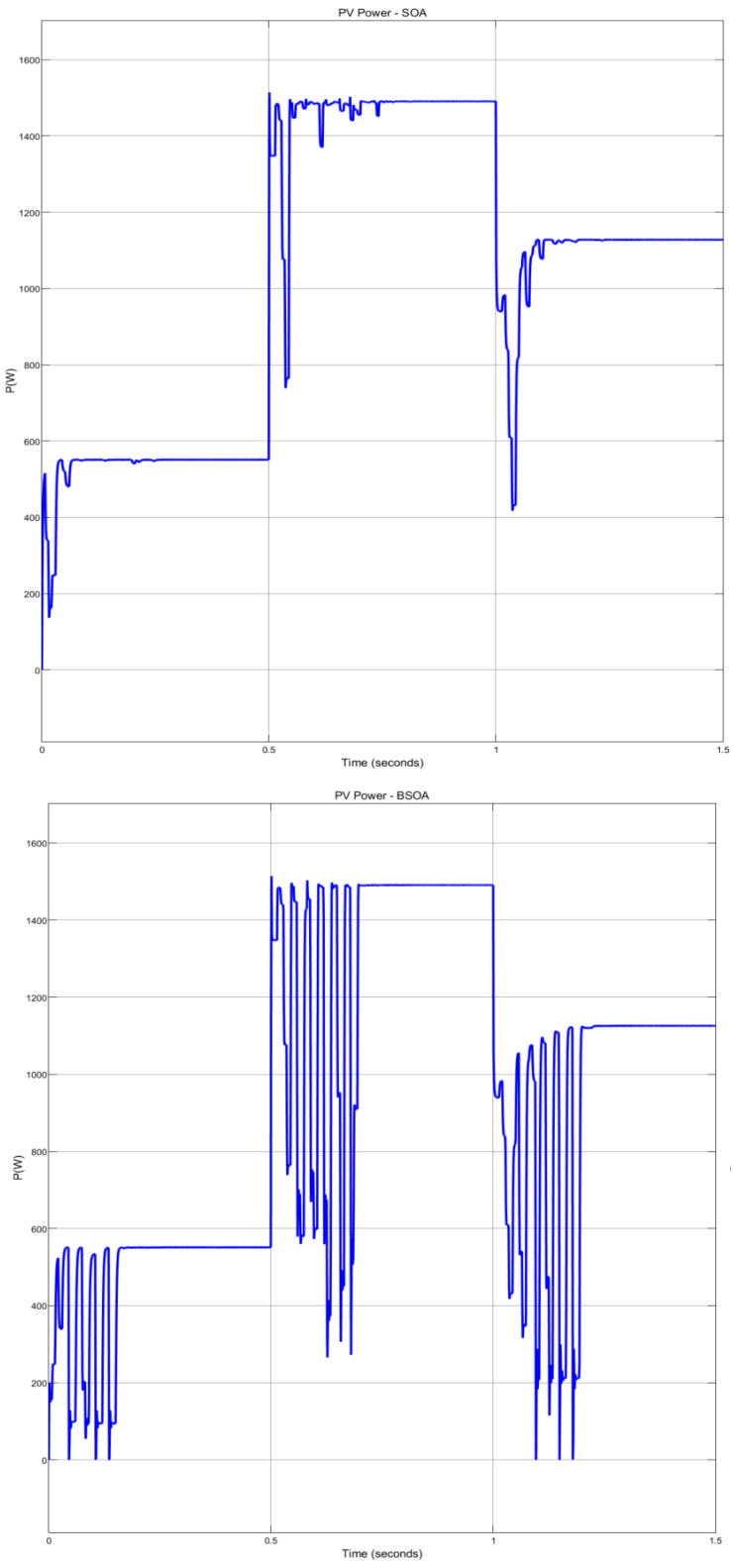

Fig 5.3 P-V Power curves for the fast-varying irradiation – case 1.

5.5.2 Non - Uniform Fast Varying irradiance.

Next figures depict the obtained power curves under partial shading conditions in cases 2 through 6, and table 5.6 provides the resulting steady state static efficiencies and tracking times.

Cases	Optimizer	GMPP (W)	Tracked Power (W)	GMPP Located	Efficiency	Convergence Time (s)
2	PSO	548.16	548.06	YES	99.97	0.285
	GWO		548.06	YES	99.97	0.258
	SOA		547.90	YES	99.94	0.255
	GSO		548.00	YES	99.97	0.166
3	PSO	703.69	703.60	YES	99.98	0.248
	GWO		703.60	YES	99.98	0.255
	SOA		703.50	YES	99.97	0.207
	GSO		703.20	YES	99.93	0.162
4	PSO	699.75	697.80	YES	99.72	0.229
	GWO		697.60	YES	99.69	0.256
	SOA		699.50	YES	99.96	0.208
	GSO		698.70	YES	99.85	0.155
5	PSO	709.13	557.60	YES	78.63	0.094
	GWO		568.40	YES	80.15	0.259
	SOA		557.60	YES	78.63	0.062
	GSO		556.50	YES	78.47	0.159
6	PSO	733.94	719.00	YES	97.96	0.221
	GWO		719.00	YES	97.96	0.254
	SOA		719.00	YES	97.96	0.125
	GSO		718.00	YES	97.82	0.159

Table 5.6. Steady State Tracking Results Under Non-Uniform Irradiance.

- **Case 2**

Irradiance levels (W/m²): 300/300/800/800/600/600/300

GMPP (W): 546.27

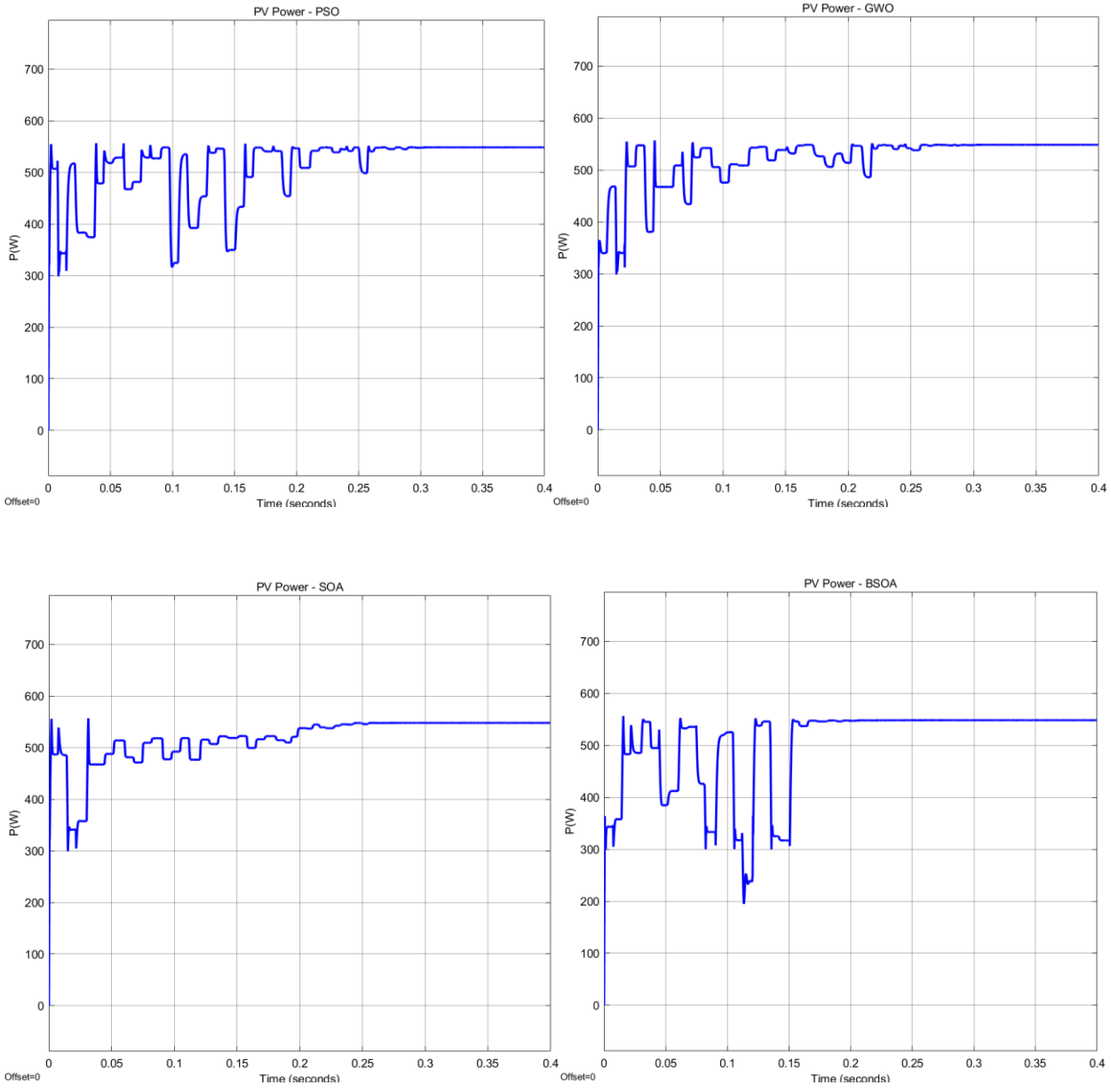

Fig 5.4 P-V Power curves for case 2.

- **Case 3**

Irradiance levels (W/m²): 1000/1000/600/300/300/800/600

GMPP (W): 703.69

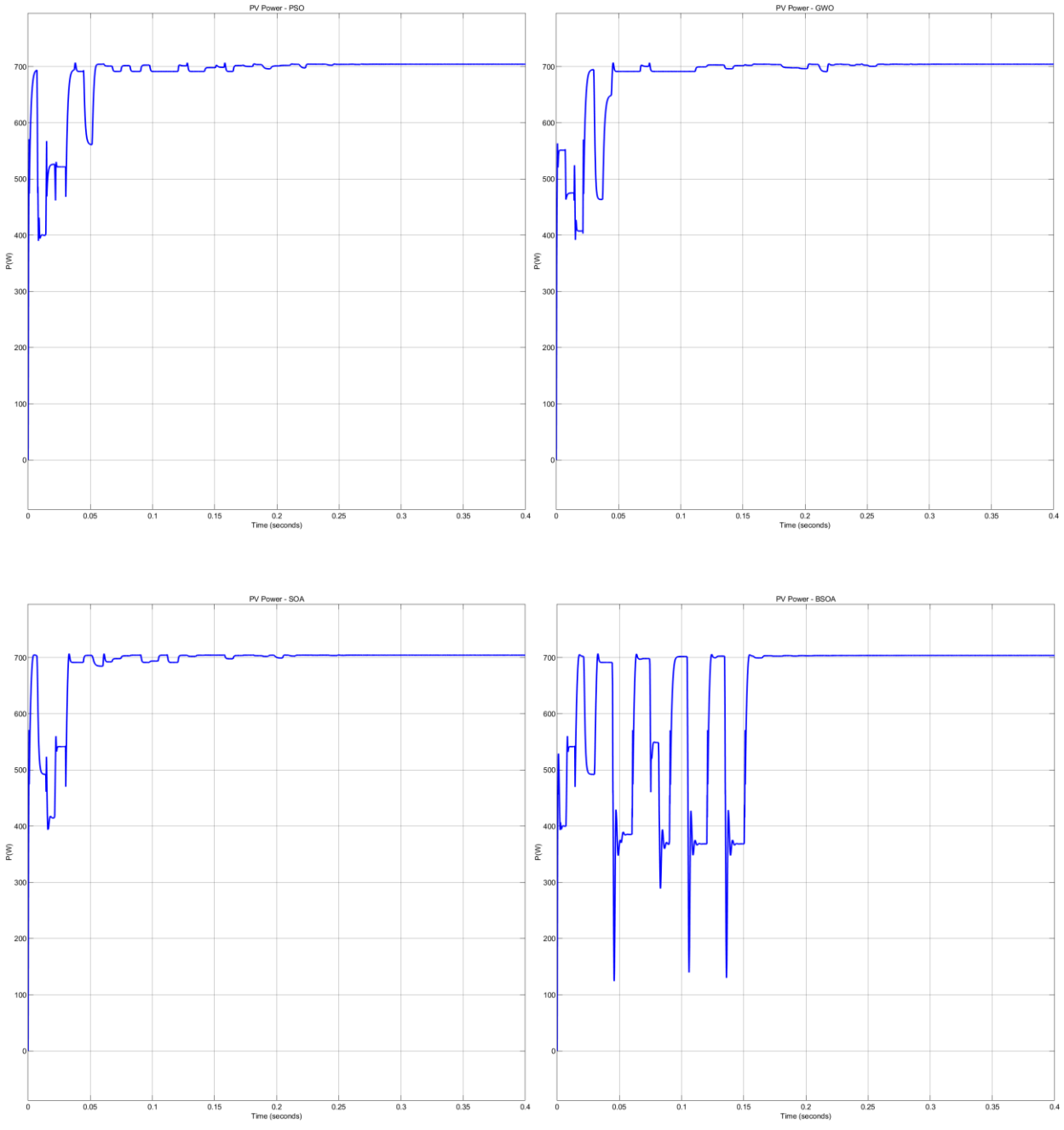

Fig 5.5 P-V Power curves for case 3.

- **Case 4**

Irradiance levels (W/m²): 1000/400/800/800/300/600/600

GMPP (W): 699.75

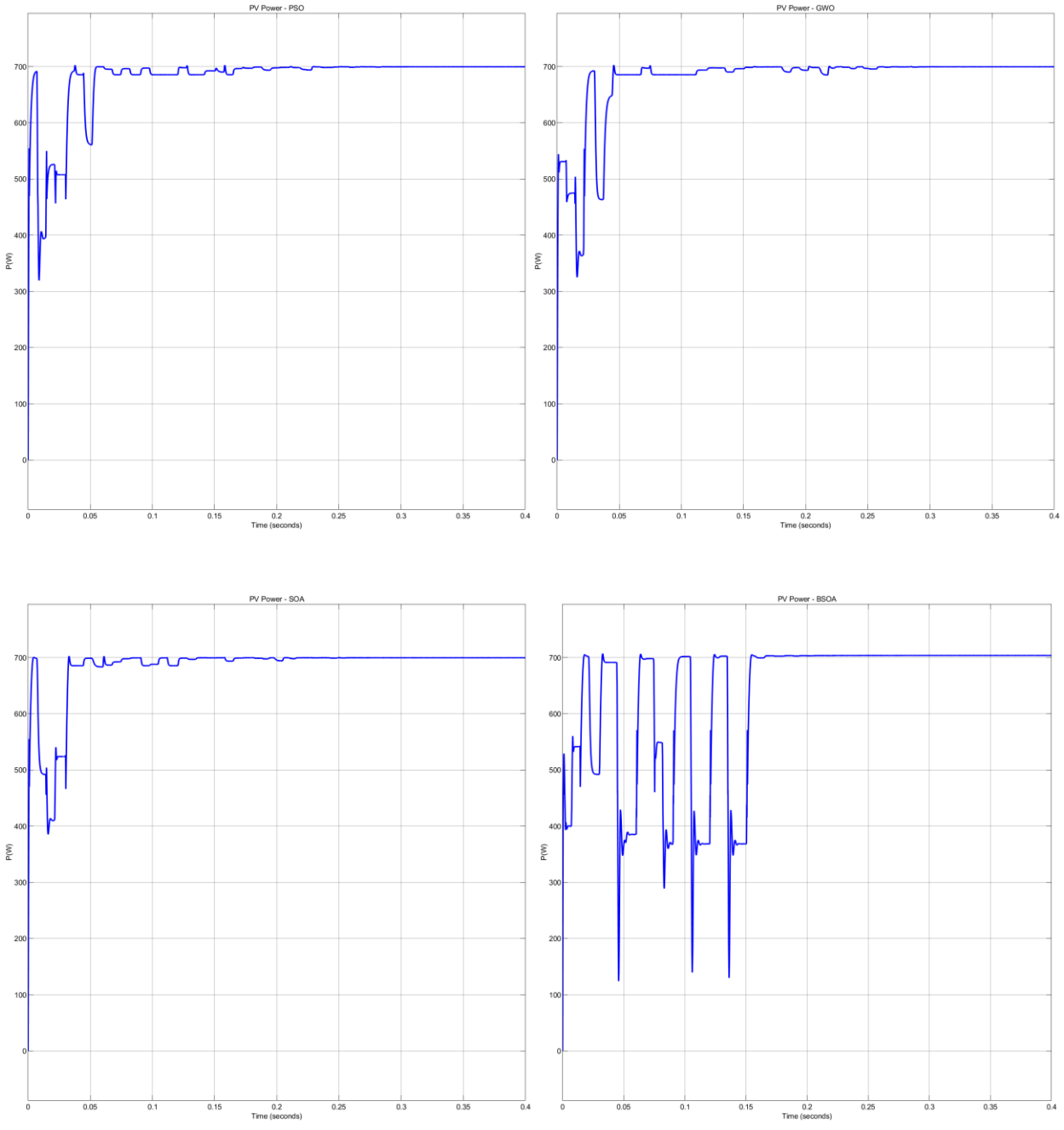

Fig 5.6 P-V Power curves for case 4.

- **Case 5**

Irradiance levels (W/m²): 1000/500/800/700/300/600/500

GMPP (W): 709.13

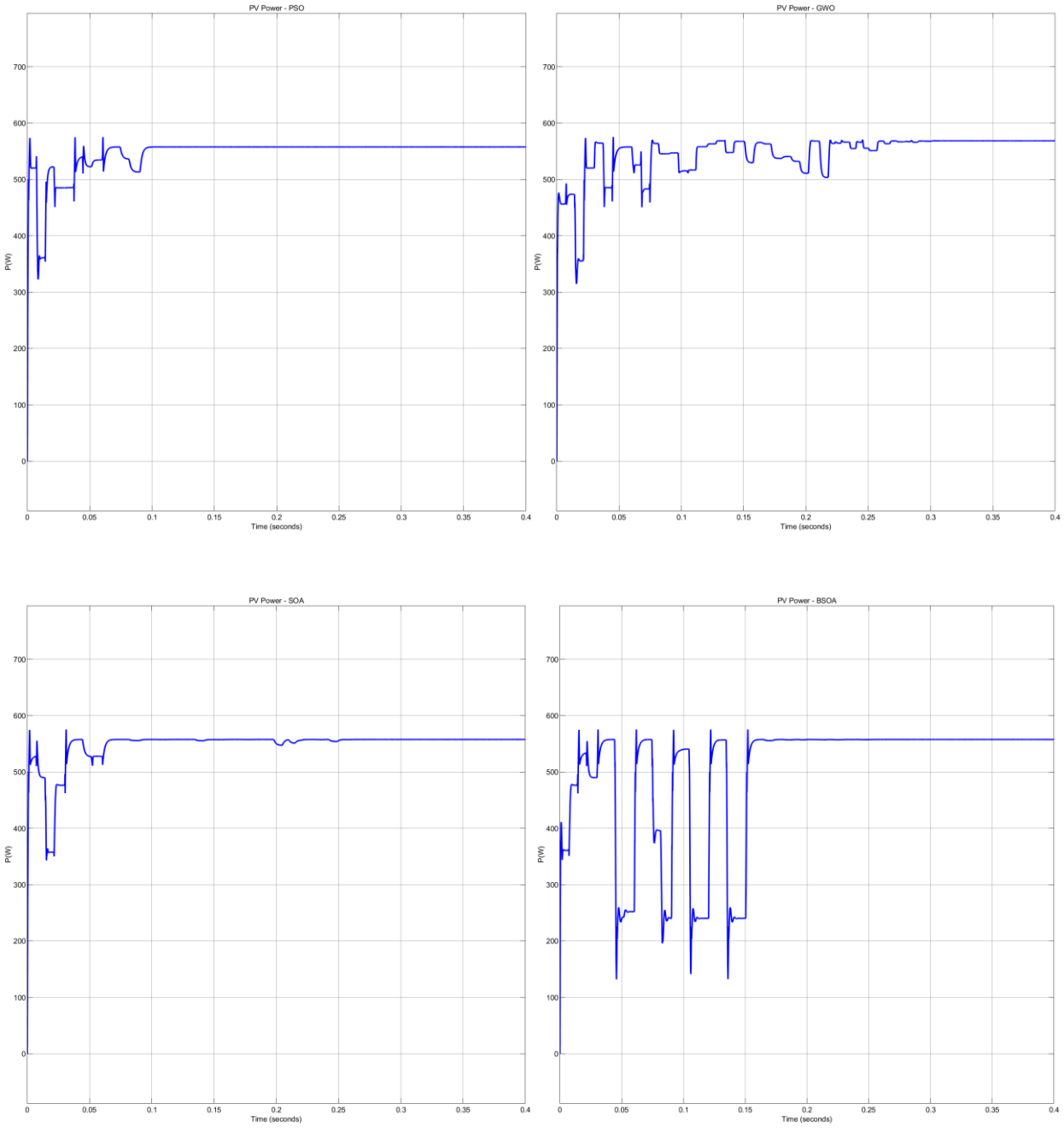

Fig 5.7 P-V Power curves for case 5.

- **Case 6**

Irradiance levels (W/m²): 1000/500/800/700/900/600/400

GMPP (W): 733.94

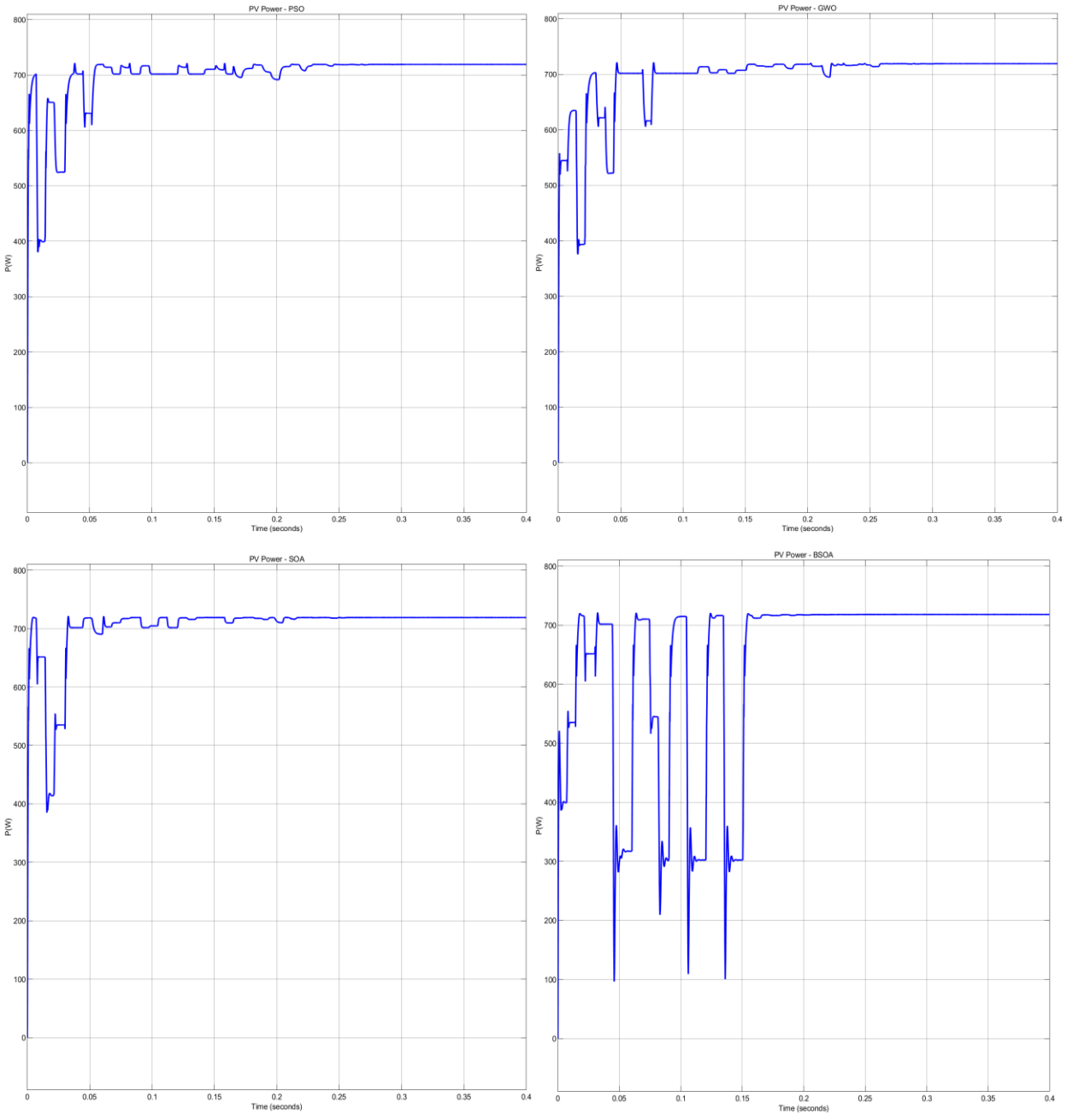

Fig 5.8 P-V Power curves for case 6.

- It can be observed that the PSO, GWO, SOA and the GSO scored almost equal efficiencies, and successfully located the GMPP associated with each case. The case 5 had the worst GMPP tracking and the worst efficiencies among all of the other cases, as the efficiency was between 78% to 80 % and did not reach the 90%.

- The GSO got the lowest power level in the fifth case at which it achieved 556.50W out of 709.13W resulting in an efficiency of 78.47% compared to the highest rank (99.88%). In the remaining shading conditions, the GSO attained perfect efficiency levels among all of the optimizers, in case 2 it achieved 548.00W out of 548.16W resulting in an efficiency of 99.97%.

- In terms of convergence speed, it can be clearly seen that the GSO is the fastest among the remaining algorithms with settling time as low as 0.155s in the 4th case up to 0.166s in the 2nd case. Using this strategy, the algorithm has high prospects of exploring promising regions rapidly, and hence undesirable areas are replaced along the optimization process, resulting in an efficacious transition from diversification into intensification.

- The SOA can be classified in the second rank with a convergence time of 0.125 second to 0.255s, which identical to the GSO.

- The GSO algorithm has succeeded in locating the global MPP region in all cases as opposed to GWO that got stagnated in a local optimum region in first case - Uniform Fast Varying irradiance- this is credited to the opposition learning scheme applied to the standard equation, which allowed the algorithm scouting different optimum regions within the search space. In terms of tracking speed, the improved algorithm surpassed its competitors in all cases, with an average convergence time of 0.16s due to the new adaptive schemes introduced to the standard factors.

5.6 Conclusion

This chapter was devoted to the evaluation of 4 metaheuristic algorithms in Maximum Power Point Tracking. Simulink and MATLAB were used to design and simulate a standalone PV system driven by an MPPT controller and subjected to various atmospheric conditions. The assessment was carried out based on the collected data obtained from 6 distinct scenarios of fast varying uniform and non-uniform irradiation, accompanied with the resulting power curves and necessary tables. The analyses of the simulation results of the studied cases, have demonstrated the effectiveness of the propound novel algorithms in handling various challenging shading patterns, and achieved the highest efficiency levels in all cases over the remaining popular stochastic algorithms. Moreover, the three proposed optimizers are characterized by fast tracking speed, this was conspicuous in the convergence time of the GSO which was 0.16s on average outperforming the remaining algorithms.

General Conclusion and Future Work

This master thesis work was devoted to the study and evaluation of the latest advancements of soft computing techniques for Maximum Power Point Tracking operation. Seagull optimization algorithm is the recent optimizer investigated in this project and assessed along with other well-known metaheuristic techniques, namely: Particle Swarm Optimization and Grey Wolf Optimization. The proposed algorithms have proved to be powerful in terms of tracking efficiency, robustness and convergence time. The comparative study revealed the fast-tracking outperformance of the Guided Seagull Optimizer over the remaining techniques, and the nearly identical outcomes obtained by the SOA and the PSO. It is worth highlighting that although the GWO was on a par with the other optimizers in terms of efficiency, some improvements need to be made, to make it faster and a better rival. Although the propound metaheuristic techniques are powerful for Maximum Power Point Tracking, the work can be further extended, and enhancements can always be made in this field. In this context, we suggest that the following points are worth investigating for future work: - A hybridization of the assessed algorithms with classical techniques can be made to reduce the convergence time of the MPPT controller. This allows exchanging between local tracking and global tracking strategies according to the solar irradiance conditions. As global maximum power point tracking takes longer time, and if the solar irradiance is uniform, it is needless to employ a global tracker, since a traditional technique like the P&O is sufficient and faster. In the other hand, if partial shading occurs, then the MPPT controller will be switched to global search using one of the proposed metaheuristic algorithms. A partial shading detection technique has to be developed for that purpose. - Evaluate the proposed algorithms under changing temperature conditions. - Realize a laboratory setup based on DSP or FPGA boards to implement and experimentally validate the feasibility of the assessed techniques in Maximum Power Point Tracking.

References:

[1] A. AZIZ, « Propriétés Electriques des Composants Electroniques Minéraux et Organiques, Conception et Modélisation d'une Chaîne Photovoltaïque Pour une Meilleure Exploitation de l'Energie Solaire », Thèse de Doctorat, Université Paul Sabatier, Toulouse III, France, 2006.

[2] Antonio Luque and Steven Hegedus, "Handbook of Photovoltaic Science and Engineering", John Wiley & Sons Ltd, 2003.

[3] W. Xiao, "A Modified Adaptative Hill Climbing Maximum Power Point Tracking (MPPT) Control Method for Photovoltaic Power Systems", thesis for degree of Master, The University of British Columbia, 2003.

[4] Akihiro Oi, "Design and Simulation of Photovoltaic Water Pumping System", theses for degree of Master, Faculty of California Polytechnic State University, 2005.

[5] J. Royer et T. Djiako et E. Schiler, B. Sadasy. 'Le pompage photovoltaïque', université d'Ottawa, 1998.

[6] OUMNAD, « Electronique Fondamentale», Ecole Mohammadia des Ingénieurs, Site Internet, http://z.oumnad.123.fr

[7] C. Hua and C. Shen, « Comparative study of peak power tracking techniques for solar storage system », IEEE Applied Power Electronics Conference and Exposition, 15-19 February, Anaheim, CA, USA, 1998.

[8] M. Z. F.Z. Zerhouni, "Optimisation d'un système à énergie verte avec validation pratique," Revue des Energies Renouvelables, vol. 11, no. N°1, p. 41– 49, 2008.

[9] A. Saadi, "Etude comparative entre les techniques d'optimisation des systèmes de pompage photovoltaïque," Université de Biskra Mémoire de Magister, 2000.

[10] Mohamed Ahmed Hassan El-Sayed, Steven B. Leeb, MAXIMUM POWER POINT TRACKING OF PV ARRAYS IN KUWAIT

[11] BOUALEM, DENDIB, "Technique conventionnelles et avanccée de pursuit MPP pour des application Mémoire de Magister, Departement photovoltaique: étude compartive, " Université Ferhat Abbes-Sétif d'éléctronique TS4/6338, 2007

[12] A. Lyes, "Etude de la connexion au réseau électrique d'une centrale photovoltaïque" UNIVERSITE MOULOUD MAMMERI DE TIZI OUZOU Mémoire de Magister, 2011.

[13] Ogundimu, Emmanuel & Akinlabi, Esther & Mgbemene, Chigbo & Jacobs, Ifeanyi. (2021). Design and Implementation of a Low-cost Irradiance -Temperature Data Logging Meter for Solar PV Applications. American Journal of Mechanical and Industrial Engineering. 6. 50-55. 10.11648/j.ajmie.20210604.12.

[14] Lesovik, Gordey & Sadovskyy, Ivan & Lebedev, Andrey & Suslov, M. & Vinokur, Valerii. (2014). H-theorem in quantum systems interacting with reservoir.

[15] Gupta, Paarth. (2020). Solar EV Chargers and Super Flow Batteries for an Efficient Electric Vehicle. International Journal of Research in Engineering and Technology. 7. 17.

[16] Al-Waeli, A.H.A., Kazem, H.A., Chaichan, M.T., Sopian, K. (2019). Introduction. In: Photovoltaic/Thermal (PV/T) Systems. Springer, Cham. https://doi.org/10.1007/978-3-030-27824-3_1

[17] Isiadinso, Ebuka. (2017). Solar Water Heating System ACS224 Ebuka Isiadinso 150144135. 10.13140/RG.2.2.35066.80323.

[18] Alanbary, Jaafer. (2018). Design and Construction of a Tracking Device for Solar Electrical Systems. The Journal of Scientific and Engineering Research. 5. 225-236.

[19] A. Lyes, "Etude de la connexion au réseau électrique d'une centrale photovoltaïque" UNIVERSITE MOULOUD MAMMERI DE TIZI OUZOU Mémoire de Magister, 2011.

[20]. M. Biswal, Mater of Technology (Rearch), "control technique for dc-dc buk converter with improved performance", National Institute of technology, Rourkela, March 2011.

[21] Philippe LETENNEUR, « Les alimentations électrique », 2003-2004.

[22] Antonio Luque and Steven Hegedus, «Handbook of Photovoltaic Science and Engineering», John Wiley & Sons Ltd, 2003.

[23] W. Xiao, « A Modifed Adaptative Hill Climbing Maximum Power Point Tracking (MPPT) Control Method for Photovoltaic Power Systems», université de Columbia, 2003.

[24] Sabri Nassim, Benkercha Rabah, Diagnostic et Détection des pannes dans le système photovoltaïque par les techniques intelligentes, Mémoire de Projet de Fin deludes, Université SAAD DAHLAB 1 de BLIDA, 2013.

[25] H. Bin, " Convertisseur continu-continu à rapport de transformation élevé pour applications pile à combustible", Thèse Doctorat de l'institut national polytechnique de Lorraine, France, 2009.

[26] H. LEQUEU – [DIV435] – Fichier: IUT-EDP-9, 2004/2005.

[27] International Journal of Engineering Practical Research 3(4) DOI:10.14355/ijepr.2014.0304.01

[28] Saad Motahhir, Abdelaziz El Ghzizal, Souad Sebti, and Aziz Derouich, Modeling of Photovoltaic System with Modified Incremental Conductance Algorithm for Fast Changes of Irradiance.

[29] J.B.R. Enslin, M.S. Wolf, D.B. Snyman, W. Swiegers, "Integrated photovoltaic maximum power point tracking converter", IEEE Transactions on Industrial Electronics, vol. 44 (6), Dec. 1997, pp.769 -773.

[30] T. Noguchi, S. Togachi, R. Nakamoto, "Short-current pulse-based maximum-powerpoint tracking method for multiple photovoltaic-and-converter module system", IEEE Trans on Industrial Electronics, vol. 49, Feb. 2002, pp. 217-223

[31] C. CABAL, “Optimisation énergétique de l’étage d’adaptation électronique dédié à la conversion photovoltaïque”, Thèse de Doctorat de l’Université Toulouse III – Paul Sabatier, France, 2008

[32] Comparative analysis of MPPT techniques for PV applications DOI:10.1109/ICCEP.2011.6036361

[33] H. Al-Atrash, I. Batarseh, K. Rustom, “Statistical modeling of DSP-based hill- climbing MPPT algorithms in noisy environments”, Conference and Exposition in Twentieth Annual IEEE Conference in Applied Power Electronics, APEC 2005, vol. 3, pp. 1773–1777.

[34] W. Xiao, W. Dunford, “A modified adaptive hill climbing MPPT method for photovoltaic power systems”, IEEE 35th annual Conference in Power electronics specialists, PESC 04. 2004, vol. 3, pp. 1957–1963.

[35] Comparison between HC, FOCV and TG MPPT algorithms for PV solar systems using buck converter April 2017 DOI:10.1109/WITS.2017.7934609 Conference: 2017 International Conference on Wireless Technologies, Embedded and Intelligent Systems (WITS)

[36] T. Tafticht, "Analyse Et Commande D'un Système Hybride Photovoltaique Eolien", Thèse de Doctorat de L'université Du Québec A Trois-Rivières (Canada), décembre 2006.

[37] W. Perruquetti and J. P. Barbot, “Sliding mode control in engineering”, Marcek dekker, Ed. New York, USA, 2002.

[38] Kennedy, J.; Eberhart, R. (1995). "Particle Swarm Optimization". Proceedings of IEEE International Conference on Neural Networks. Vol. IV. pp. 1942–1948. doi:10.1109/ICNN.1995.488968.

[39] AA Particle Swarm Optimization-Based Maximum Power Point Tracking Algorithm for PV Systems Operating Under Partially Shaded Conditions IEEE Transactions on Energy Conversion DOI: 10.1109/TEC.2012.2219533

[40] Chapter 3 - Impacts of metaheuristic and swarm intelligence approach in optimization https://doi.org/10.1016/B978-0-323-85117-6.00008-X

[41] Barka Nour-Eddine, "Amélioration des Performances de Contrôle D’un Système Photovoltaïque par les Méthodes Métaheuristques", Mémoire de Magister, Université d’El-oued, 2013.

[42] Grey Wolf Optimizer, Seyedali Mirjalili, https://doi.org/10.1016/j.advengsoft.2013.12.007

[43] L. D. Mech, "Alpha status, dominance, and division of labor in wolf packs," Canadian Journal of Zoology, vol. 77, pp. 1196-1203, 1999.

[44] S. Mirjalili, A. H. Gandomi, S. Z. Mirjalili, S. Saremi, H. Faris, and S. M. Mirjalili, “Salp Swarm Algorithm: A bio-inspired optimizer for engineering design problems,” Advances in Engineering Software, vol. 114, pp. 163–191, Dec. 2017

[45] H. Faris, S. Mirjalili, I. Aljarah, M. Mafarja, and A. A. Heidari, “Salp Swarm Algorithm : Theory, Literature Review, and Application in Extreme Learning Machines,” in Nature-Inspired Optimizers, S. Mirjalili, J. Song Dong, and A. Lewis, Eds. Cham : Springer International Publishing, 2020, vol. 811, pp. 185–199.

[46]A Salp-Swarm Optimization based MPPT technique for harvesting maximum energy from PV systems under partial shading conditions https://doi.org/10.1016/j.enconman.2020.112625

[47] Harmonized salp chain-built optimization DOI:10.1007/s00366-019-00871-5

[48] https://onekindplanet.org/animal/seagull/

[49] Dhiman, Gaurav & Chahar, Vijay. (2018). Seagull Optimization Algorithm: Theory and its Applications for Large Scale Industrial Engineering Problems. Knowledge-Based Systems.

[50]S. M. Macdonald and C.F. Mason. Predation of migrant birds by gulls. Brit. Birds, 66:361–363, 1973.